RSC Advances

PAPER

View Article Online
View Journal | View Issue

Cite this: *RSC Adv.*, 2024, **14**, 24725

Sulfonamide based pyrimidine derivatives combating *Plasmodium* parasite by inhibiting falcipains-2 and falcipains-3 as antimalarial agents†

Abdur Rahman,‡[a] Shazia Anjum,‡[a] Jaimin D. Bhatt,[b] Bharat C. Dixit,[b] Anju Singh,[a] Sabiha khan,[a] Sadaf Fatima,[a] Tarosh S. Patel *[b] and Nasimul Hoda *[a]

In this report, we present the design and synthesis of a novel series of pyrimidine-tethered spirochromane-based sulfonamide derivatives aimed at combating drug resistance in malaria. The antimalarial effectiveness of these compounds was assessed *in vitro*. Structural validation of the synthesized compounds was conducted using mass spectrometry and NMR spectroscopy. Strong antimalarial activity against CQ-sensitive (3D7) and CQ-resistant (W2) strains of *Plasmodium falciparum* was demonstrated by the majority of the compounds. Notably, compounds **SZ14** and **SZ9** demonstrated particularly potent effects, with compound **SZ14** showing IC_{50} values of 2.84 μM and **SZ9** 3.22 μM, indicating single-digit micromolar activity. The compounds exhibiting strong antimalarial activity were assessed through enzymatic tests against the cysteine protease enzymes of *P. falciparum*, falcipain-2 and falcipain-3. The results indicated that **SZ14** and **SZ9** inhibited *Pf*FP-2 (IC_{50} values: 4.1 and 5.4 μM, respectively), and *Pf*FP-3 (IC_{50} values: 4.9 and 6.3 μM, respectively). To confirm the compounds' specificity towards the parasite, we investigated their cytotoxicity against Vero cell lines, revealing strong selectivity indices and no significant cytotoxic effects. Additionally, *in vitro* hemolysis testing showed these compounds to be non-toxic to normal human blood cells. Moreover, predicted *in silico* ADME parameters and physiochemical characteristics demonstrated the drug-likeness of the synthetic compounds. These collective findings suggest that sulfonamide derivatives based on pyrimidine-tethered oxospirochromane could serve as templates for the future development of potential antimalarial drugs.

Received 14th June 2024
Accepted 29th July 2024

DOI: 10.1039/d4ra04370g

rsc.li/rsc-advances

1. Introduction

Malaria is a severe deadly infective disease that causes illness and deaths across many tropical and subtropical countries.[1,2] Plasmodium parasites are transmitted to humans by the bites of infected female Anopheles mosquitoes.[3] The World Health Organization (WHO) estimated 249 million cases and 608 000 deaths from malaria in 2022 with an increase of 5 million new cases and a slight decline in malarial deaths from 2021, indicating that malaria is still difficult to control.[4] Artemisinin-based combination therapies (ACTs) are an increasingly common treatment for preventing malaria. However, the effectiveness of ACTs is reduced gradually on the grounds of the emergence of resistance against partner medications, especially in Southeast Asia[5,6] and presently in Sub-Saharan Africa.[7] Consequently, these situations have prompted medicinal chemists to design and develop novel inhibitors with new modes of action targeting several crucial enzymes that exhibit a vital role in the parasitic life cycle to tackle the emergence of drug resistance to some extent.

Cysteine protease is one of the most promising chemotherapeutic targets for various infectious diseases caused by parasites which include *Leishmania*, *Entamoeba histolytica*, *Toxoplasma gondii*, *Trypanosoma brucei*, *Cryptosporidium* and *T. cruzi*.[8–11] Cysteine protease enzymes in the *Plasmodium* genus play an important role in parasite organisms to catalyze the host hemoglobin deterioration in the acidic food vacuole, thereby offering essential amino acids for the survivability and development of malaria parasites.[12,13] Four subtypes of falcipains in plasmodium are identified: falcipains-1, falcipains-2, falcipains-2′, and falcipains-3. Gene-knockout investigations and the FPs expression by erythrocytic parasites have shown that FP-2 and FP-3 found a 68% homology, which is likely important in regulating the parasite's erythrocytic stage.[14,15] However, FP-1 develops during the parasite's schizont/merozoite stage and does not seem necessary for the malaria parasite during its erythrocytic stage.[15] The study by the Sijwali group

[a]*Drug Design and Synthesis Lab., Department of Chemistry, Jamia Millia Islamia, Jamia Nagar, New Delhi 110025, India. E-mail: nhoda@jmi.ac.in; Fax: +0091-11-26985507; Tel: +0091-9910200655*

[b]*Chemistry Department, V. P. & R. P. T. P Science College, Affiliated to Sardar Patel University, Vallabh Vidyanagar 388120, Gujarat, India. E-mail: tarosh_patel@yahoo.com; Tel: +91-2692-230011#31*

† Electronic supplementary information (ESI) available. See DOI: https://doi.org/10.1039/d4ra04370g

‡ Equal contribution.

demonstrated that disruption in the FP-2 gene has a potential impact on the degradation of hemoglobin. However, the disruption of the FP-2′ has no impact on the degradation of hemoglobin, and the FP-3 was established to be crucial for the development of the erythrocytic parasite.[16] Therefore, efforts to synthesize drugs targeting FP-2 were made because it seems to serve as the primary hemoglobinase, breaking down hemoglobin at several sites and contributing to the degradation of the proteins that make up the membrane of an erythrocyte skeletal system. For FP-2 and FP-3, several peptides and non-peptide inhibitors, including leupeptin and E64, have been identified; however, neither of these individuals has reached clinical trials because of poor bioavailability and toxicological profile.[14,17–21] Therefore, inhibition against cysteine protease particularly for falcipains could lead to the arrest of parasitic growth, highlighting an attractive target for antimalarial drug development.[22–24]

Thus, two distinct biologically active pharmacophores were hybridized to develop single and potent hybrid antimalarial agents. This developed hybrid molecule could have the potential of low risk of drug resistance, enhanced solubility, and lower toxicity than the parent pharmacophore.[25,26] In addition, the two partner medications may interact more effectively with the target protein and have greater activity when an appropriate linker links their active moieties together than when they are administered individually.[27] The pharmacokinetic characteristics of a hybrid medication are therefore simpler to forecast and control when compared to two separate medications.[28] Therefore, expanding our fascinating results with molecular hybrids for developing new malarial medications, herein we introduced a rational design of a hybrid set of pyrimidine-tethered spirocyclic chromane as antimalarial agents according to various pharmacophore combination approaches.

1.1. Design strategy

Pyrimidines, a heterocyclic nitrogen-containing scaffolds that are commonly found in several natural bioactive products and have diverse biological activities such as antitumor, antitubercular, anti-allergic, antipyretic, antibacterial, anti-inflammatory, and antimalarial activities.[29,30] Pyrimethamine, a derivative of pyrimidine, was used to treat malaria, targeting the enzyme DHFR.[31] Kareem *et al.*[32] have explored the optimization of pyrimidine-based compounds that demonstrated *in vitro* anti-plasmodial activity and act as dual inhibitors of plasmodial *Pf*GSK3/*Pf*PK6. Similarly, Coteron *et al.*[33] have developed 5-substituted-2-cyanopyrimidine-based derivatives (Fig. 1) as cysteine protease inhibitors particularly for falcipains (FP-2 and FP-3) of the *Plasmodium* parasite, showing significant activity. Recent studies[34–36] established that pyrimidine is an attractive bioactive scaffold in the development of new antimalarial agents.

The incorporation of spirocyclic scaffolds has been found in recently approved drugs which has led to the escape from flatland to provide less planar molecule with improved potency.[37] In addition, the spirocyclic compound with a well-defined three-dimensional arrangement has a greater possibility of being the drug candidate appearing in clinical trials.[38] A recent investigation by Brindisi *et al.*[39] presented that spirocyclic compounds possessed improved antimalarial activity. Spirocyclic indolone NITD609 developed by Turner *et al.* has demonstrated remarkable antimalarial activity, inhibiting *Pf*ATP4, for which phase II clinical trials have been carried out on adults with uncomplicated malaria led by *P. falciparum* in sub-Saharan Africa.[40] Similarly, spirocyclic chromane-based analogs (Fig. 1) have emerged as new pharmacophores with potent antimalarial activity.[41]

Sulfonamide-based derivatives exhibited diverse biological activities in medicinal chemistry which include fungicidal,

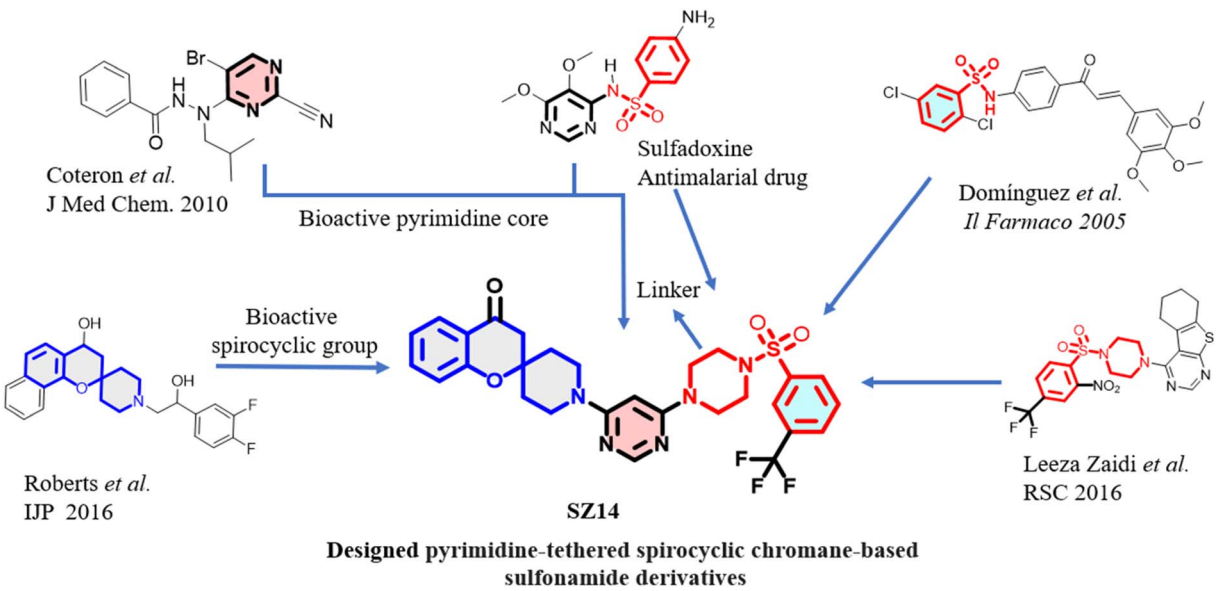

Fig. 1 Rationale for the design of sulfonamide derivatives based on pyrimidine-tethered spirocyclic chromane.

nematicidal, and bactericidal activities.[42] Several research groups have investigated the antimalarial activity of sulphonamide-containing compounds.[43–45] Domínguez *et al.*[46] synthesized the chalcone-based aryl sulfonamide derivatives (Fig. 1) for the inhibition of beta-hematin formation and evaluated their activity against the *Plasmodium* parasite. Similarly, Leeza Zaidi *et al.* [47] developed thienopyrimidine-based aryl sulphonamide derivatives (Fig. 1) which have antimalarial activity in the micromolar range. In addition, a combination of pyrimethamine-sulfadoxine which is a derivative of sulfonamide is still effective as a curative measure of malarial disease in pregnant women in Tanzania, indicating the importance of developing new sulphonamide-based derivatives to cure malaria.[48] Additionally, recent reports[49–51] described the antimalarial advancements and hydrophilicity that occur due to the incorporation of the piperazine ring in synthetic compounds and provided an easy way to understand the rationale behind the ring's introduction.

Thus, by keeping all these factors in mind, we disclosed the outcomes of our recent work comprising a series of new pyrimidine-tethered spirocyclic chromane-based sulphonamides and their antiplasmodial activity were examined toward drug-susceptible (3D7) strain and drug resistance (W2) strain of *P. falciparum*. Furthermore, the molecules with good antimalarial efficacy were tested for enzymatic assay (FP-2 and FP-3) followed by cytotoxicity and hemolysis assay. Our findings indicate that the newly synthesized compounds could be utilized as research models and are appropriate for use in future drug development.

2. Results and discussions

2.1. Synthetic chemistry

A linear synthetic method was applied to synthesize the design molecules (**SZ1–SZ14**), sketched in (Scheme 1). The synthesis began with preparing the intermediate (**1**) by treating the commercially available -*ortho*-hydroxy acetophenone and 1-boc-piperidone-4-one by known literature procedure. Then intermediate (**1**) was subjected to deprotection of the Boc group to gain the nucleophilic intermediate (**2**) using the standards deprotection conditions, TFA in the presence of solvent dichloromethane.[41] Further, commercially available 4,6-dichloropyrimidine was reacted with the intermediate compound (**2**) along with triethylamine to synthesize the intermediate compound (**3**) which was subsequently treated with anhydrous piperazine and K_2CO_3 to get the final

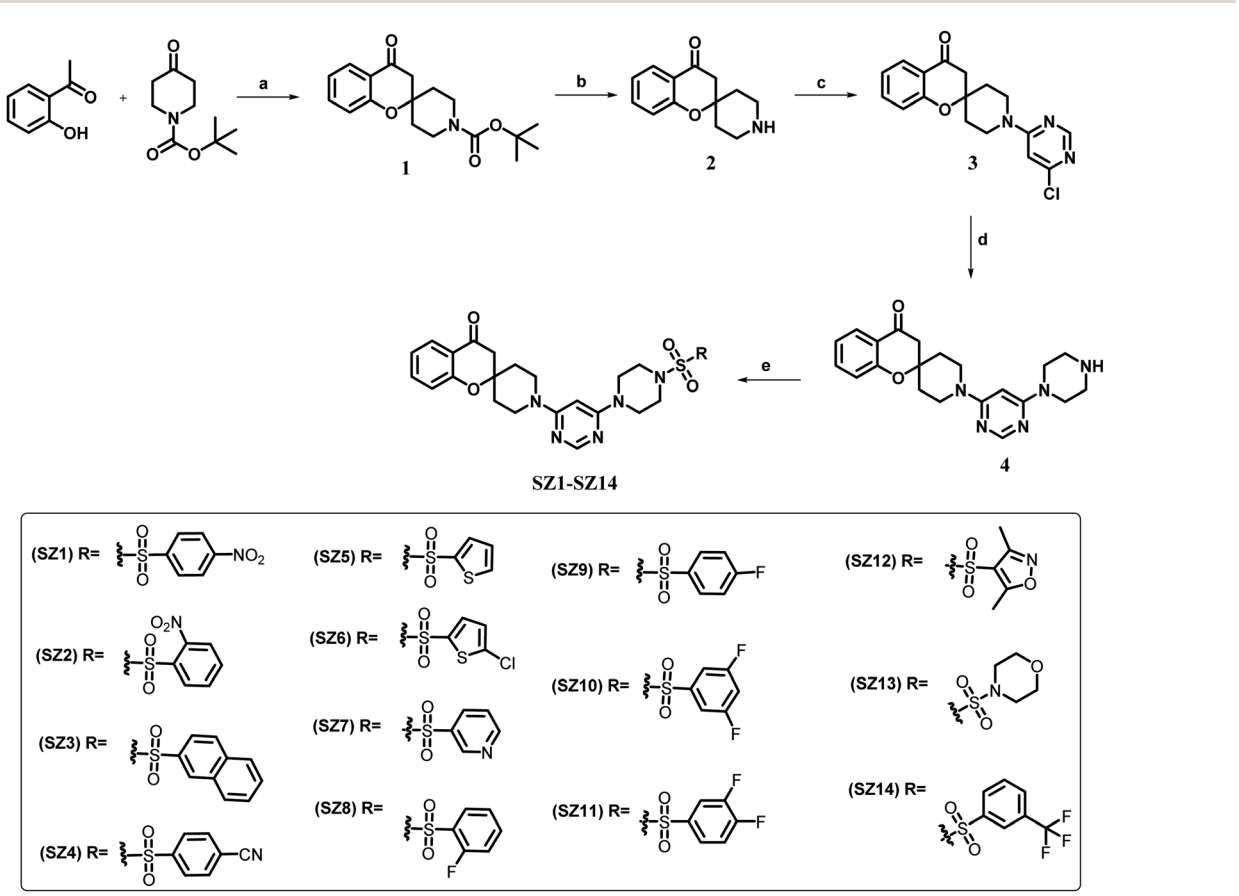

Scheme 1 Synthesis of sulfonamide derivatives based on pyrimidine-tethered spirochromane targeted compounds (SZ1–SZ14)[a]. [a]Reagent and conditions: (a) pyrrolidine, methanol, reflux at 80 °C, 6–8 h, 77% yield; (b) trifluoroacetic acid (TFA), DCM, r.t., 2 h, 73% yield; (c) 4,6-dichloropyrimidine, triethylamine, dry THF, rt, overnight, 46% yield; (d) anhydrous piperazine, K_2CO_3, dioxane, reflux at 80 °C, 10 h, 70% yield; (e) various sulfonyl chlorides, dried methanol, 0 °C, 8 h, 54–70% yield.

Table 1 The IC_{50} values for every tested entity (SZ1–SZ14) against the parasite strains 3D7 and W2 of *Plasmodium* and the corresponding resistance index (RI). The inhibition results are the mean of three separate experiments with the standard deviation

	*Pf*3D7	*Pf*W2	
Compounds	IC_{50} (μM)	IC_{50} (μM)	Resistance index (RI)[a]
SZ1	14.76 ± 0.24	>15	ND
SZ2	18.12 ± 0.43	>15	ND
SZ3	25.24 ± 0.35	>15	ND
SZ4	6.33 ± 0.29	14.36 ± 0.16	0.44
SZ5	7.45 ± 0.37	13.28 ± 0.19	0.56
SZ6	6.68 ± 0.09	4.76 ± 0.25	1.40
SZ7	7.97 ± 0.33	5.64 ± 0.18	1.41
SZ8	5.61 ± 0.42	8.12 ± 0.37	0.69
SZ9	**3.22 ± 0.07**	**3.89 ± 0.23**	**0.83**
SZ10	4.55 ± 0.34	6.67 ± 0.16	0.68
SZ11	3.92 ± 0.25	5.58 ± 0.19	0.70
SZ12	8.46 ± 0.28	>15	ND
SZ13	22.21 ± 0.36	>15	ND
SZ14	**2.84 ± 0.21**	**3.12 ± 0.14**	**0.91**
CQ[b]	0.018 ± 0.002	0.051 ± 0.001	0.35
PYR[b]	0.015 ± 0.0002	129.0 ± 11.3	0.00012

[a] ND = not determined. [b] Reported earlier.[52]

intermediate compound (**4**). Finally, the intermediate (**4**) was treated with various commercially available sulfonyl chlorides to furnish the target compounds (**SZ1–SZ14**) in good yield.

The final compounds were purified by column chromatography and nuclear magnetic resonance spectroscopy (NMR) was utilized to determine their structural elucidation. Correlated results are included in the supplemental data in Fig. S2–S17.† Moreover, the molar mass of the synthesized hybrids was validated using high-resolution mass spectrometry (HRMS), and it was discovered that the predicted mass and the molar mass matched well. The Fig. S18–S22 in the ESI† provides their projected molecular weight.

2.2. *In vitro* biological studies

2.2.1. *In vitro* test for antimalarial efficacy. The synthesized molecules were tested for *in vitro* antiplasmodial efficacy with both the 3D7 strain susceptible to chloroquine (CQ) and W2 strain resistant to chloroquine (CQ) of *Plasmodium falciparum* while tested results (IC_{50} values) are depicted in (Table 1). The IC_{50} values reported demonstrated the dosages of the compounds under investigation in μM required for halting 50% of the parasite development. The reported data is made up of the mean results from the triple experiments. All the molecules exhibited excellent to modest antiplasmodial efficacy against the 3D7 CQ-susceptible strain of *P. falciparum*. Molecules **SZ9**, **SZ10**, **SZ11**, and **SZ14** were highly effective against the *Pf*3D7 CQ-susceptible strain. Molecule **SZ14** (IC_{50} of 2.84 μM) displayed promising potency which was more potent than molecules **SZ9**, **SZ10**, and **SZ11** having IC_{50} values of 3.22 μM, 4.55 μM, and 3.92 μM respectively, with the exception that their effects differed significantly from the actions of the reference medications pyrimethamine and chloroquine. Molecules **SZ4**, **SZ5**, **SZ6**, **SZ7**, **SZ8**, and **SZ12** showed modest antimalarial efficacy with IC_{50} values of 6.33 μM, 7.45 μM, 6.68 μM, 7.97 μM, 5.61 μM, and 8.46 μM respectively while, molecules **SZ1**, **SZ2**, **SZ3**, and **SZ13** showed lowest antimalarial efficacy having IC_{50} values of 14.76 μM, 18.12 μM, 25.24 μM, and 22.21 μM respectively which was almost 5-fold reduced than potent molecules **SZ9**, **SZ10**, **SZ11** and **SZ14**. Interestingly, molecule **SZ14** was found the most active compound for the *Pf*W2 strain, with an IC_{50} of 2.84 μM. The molecules **SZ6**, **SZ7**, and **SZ8** were the modestly active molecule having an IC_{50} of 4.76 μM, 5.64 μM, and 8.12 μM respectively while the rest of the molecules demonstrated antiplasmodial activity with IC_{50} above 13 μM. In addition, the structure–activity relationship (SAR) between the synthesized molecules was established and it was found that the benzene ring with comparatively less electron withdrawing group exhibited the best result among the pyridine, thiophene, isoxazole, and morpholine ring (Table 1). Further, it was observed that the **SZ9** molecule with a *para* –F group showed potent activity in comparison to **SZ10** with difluoro both at the *meta* positions and **SZ11** bearing difluoro at the meta and *para* positions whereas **SZ1** and **SZ2** with nitro group at *para* and *ortho* position of benzene ring respectively exhibited activity with IC_{50} more than 14 μM against both the strain (Table 1). The **SZ4** compound bearing cyano (–CN) at the *para* position showed enhanced activity with the *Pf*3D7 strain with IC_{50} 6.33 μM. Interestingly, the compound **SZ14** molecule with $-CF_3$ at the meta position of the benzene ring exhibited the highest potency among the series of compounds against both the strains (*Pf*3d7 and *Pf*W2) which have fragment-based similarity with 4-pyridone-based antimalarial inhibitors and FDA approved drug tafenoquine.[53,54] Therefore, it was noticed that only less electron withdrawing or electron donating group increases the activity of the compound by providing suitable electron cloud densities on the benzene ring, resulting in proper interaction of the ligand with the active site residues of the target enzyme. The compound **SZ14** exhibited a resistance index (RI) of 0.91 ≅ 1, which is the ratio of the IC_{50} value of the CQ-resistant strain to the IC_{50} value of the CQ-sensitive strain. This value was superior to CQ (RI = 0.35), suggesting that the **SZ14** hybrid exhibited potency against both sensitive and resistant strains of *P. falciparum*.

2.2.2. *In vitro* enzyme inhibition against FP-2 and FP-3. An enzymatic experiment was executed implementing the

Table 2 The results of enzyme inhibition of the test (SZ1–SZ14) compound against FP-2 and FP-3 of *P. falciparum* parasites[a]

	Enzyme inhibition	
Compounds	Falcipain-2 (IC_{50} μM)	Falcipain-3 (IC_{50} μM)
SZ9	**4.9 ± 1.3**	**6.3 ± 1.2**
SZ10	7.2 ± 1.8	8.8 ± 1.5
SZ11	6.5 ± 1.6	8.0 ± 1.4
SZ14	**4.1 ± 1.1**	**5.4 ± 0.7**
E-64	54.4 ± 5.6[b]	116.2 ± 8.7[b]

[a] The depicted results are mean of triplicate. [b] IC_{50} value in nM.

Table 3 Cytotoxicity of the selected entities (**SZ9**, **SZ10**, **SZ11**, and **SZ14**) against Vero cells and A5489 cells along with their respective selectivity index (SI)[a]

	*Pf*3D7	*Pf*W2	Cytotoxicity (IC_{50} μM)		Selectivity index (SI) with *Pf*3D7 strain		Selectivity index (SI) with *Pf*W2 strain	
Compounds	IC_{50} (μM)	IC_{50} (μM)	Vero cell	A5489	Vero cell	A5489	Vero cell	A5489
SZ9	3.22 ± 0.07	3.89 ± 0.23	N.C.	78.47 ± 2.76	310.55	24.36	257.06	20.17
SZ10	4.55 ± 0.34	6.67 ± 0.16	N.C.	122.46 ± 3.39	219.79	26.91	149.92	18.35
SZ11	3.92 ± 0.25	5.58 ± 0.19	N.C.	94.15 ± 2.97	255.10	24.01	179.21	16.87
SZ14	2.84 ± 0.21	3.12 ± 0.14	N.C.	66.22 ± 2.14	352.11	23.31	320.51	21.22

[a] N.C. denotes no cytotoxicity noticed up to 1000 μM; SI (selectivity index) = ratio of cytotoxicity assay's IC_{50} value and the inhibitory concentration against the specific strains.

outcomes of the anti-malarial testing against the *Pf*W2 strain to evaluate the effectiveness of the four drugs in preventing the development of falcipains. Throughout the investigation, the widely available cysteine protease inhibitor E-64 was utilized as a standard reference (Table 2) summarizes the obtained IC_{50} values.

The results demonstrated that molecules **SZ10** (FP-2 = 7.2 μM and FP-3 = 8.8 μM) and **SZ11** (FP-2 = 6.5 μM and FP-3 = 8.0 μM) were least potent against the two enzymes, FP-2 and FP-3 as they had the lowest effectiveness against the *Pf*3D7 strain while molecule **SZ9** (FP-2 = 4.9 μM and FP-3 = 6.3 μM) and **SZ14** (FP-2 = 4.1 μM and FP-3 = 5.4 μM) was most potent against both FP-2 and FP-3 enzymes among others. Additionally, the obtained IC_{50} values from this *in vitro* enzymatic assay supported the validation of the preliminary assay result against 3D7 and W2 strains. Consequently, the results indicated that the molecule was considered to be a potent inhibitor of falcipains belonging to enzyme cysteine proteases, and the **SZ14** molecule may serve as a lead molecule against the plasmodium parasite.

2.2.3. Cytotoxicity evaluation. Selected compounds (**SZ9**, **SZ10**, **SZ11**, and **SZ14**) were also tested for cytotoxicity evaluation with the normalized two mammalian cell lines (lung cancer A5489 and non-cancerous Vero cells) to check whether the cited activities caused by their cytotoxicity or antiplasmodial effectiveness (Table 3). As is evident, the chosen test compounds were discovered to be somewhat cytotoxic to malignant cells but nontoxic to Vero cells even at a dosage of 1000 μM. Molecule **SZ14** was the highest active as an antimalarial (FP-2 = 4.1 μM and FP-3 = 5.4 μM) with the lowest cytotoxic effect (66.22 μM) against the lung cancer A5489 cell line, giving rise to a strong selectivity of the malaria parasite over human cells and an excellent safety index. On the contrary, Molecule **SZ10** was the lowest active as an antimalarial (FP-2 = 7.2 μM and FP-3 = 8.8 μM) with the highest cytotoxic effect (122.46 μM) against the lung cancer A5489 cell line, demonstrating a low selectivity for the *Plasmodium* parasite in comparison to human cells and a low safety index. The remaining compounds exhibited moderate to low cytotoxicity (Table 3). Additionally, the selectivity indices also suggested that the molecule has anticancer properties, indicating compound could be further developed as an antimalarial agent as well as an anticancer agent.

2.2.4. Impact of the compound on parasitic growth. The Malaria parasite's hemoglobin-degrading mechanism depends on hemoglobinases, frequently recognized as the Falcipains (FP2 and FP3) enzymes.[55] Based on the current study, *Pf*FP2 appears during the trophozoite stage, whereas *Pf*FP3 develops during the late trophozoite stages or early schizont.[56] It is widely acknowledged that the abnormalities of morphology and growth, especially those of the food vacuole, are caused by falcipains inhibitors. [23,57] Therefore, the impact of the compounds on *Plasmodium falciparum*'s morphology and growth was carefully examined. The malaria parasite initiates its erythrocytic growth when a merozoite invades an erythrocyte. Over 48 hours, the parasite develops through the phases of ring, trophozoite, and schizont. The effects of **SZ9**, **SZ10**, **SZ11**, and **SZ14** active entities on erythrocytic growth were investigated. The ring-stage parasites were exposed to the DMSO as control and tested chemicals (3 × IC_{50} concentration). The parasites' Geimsa-stained smears were examined after 24 and 48 hours (Fig. 2) The DMSO-treated cultures grew and generated new rings as predicted after 48 hours, as demonstrated (Fig. 2). The growth of the parasite culture administered with the entities **SZ9**, **SZ10**, **SZ11**, and **SZ14** appears to have been stopped at the early trophozoite stage. However, neither of the parasite cultures showed signs of fresh ring development after 48 hours. According to Rosenthal *et al.*'s study,[58] lipophilic substances are easier for the parasite's feeding vacuole to reach than less lipophilic counterparts. Consequently, variations in lipophilicity may account for the slight variations in the effectiveness of different compounds on the growth of parasites.

2.2.5. Hemolysis assay. The entities (**SZ1–SZ14**) have been scrutinized for their hemolytic effects on erythrocytes from humans at a dose of 100 μM using saponin to determine their biocompatibility with uninfected human red blood cells (RBCs). The presence-tested chemicals were incubated with RBCs, with chloroquine as a positive control. On erythrocytes, saponin lysis has been reported. All of the compounds exhibited less than 10% cell lysis at a dose of 100 μM. **SZ14** showed less toxicity followed by **SZ9**, **SZ11**, and **SZ10** which, in contrast to the remaining chemicals, happens to be the least toxic. Moreover, at 100 μM, the compounds' hemolysis of red blood cells was comparable to that induced by DMSO or chloroquine, suggesting that these compounds' antimalarial action was

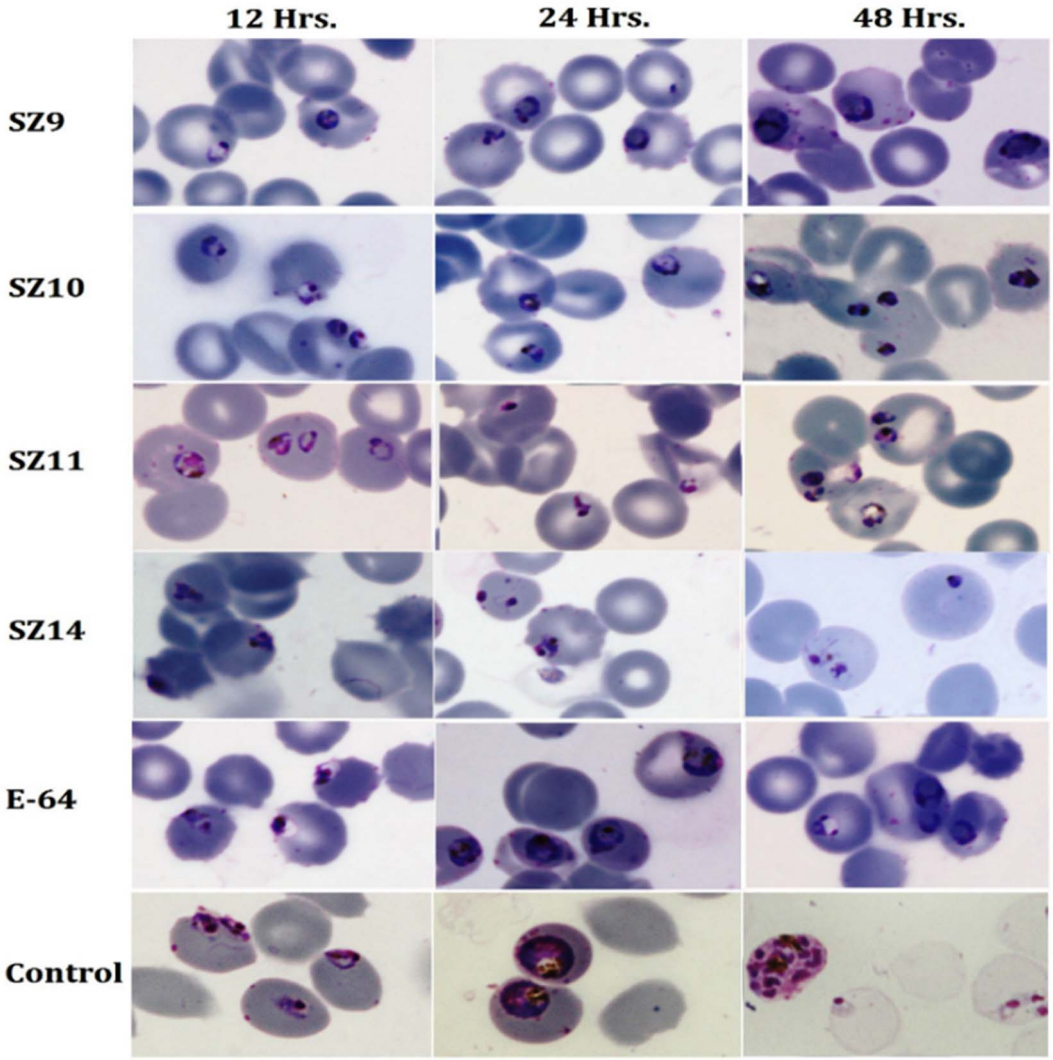

Fig. 2 Compound's impact on the growth and morphology of *P. falciparum*.

selective. These findings imply that the investigated drugs' antiplasmodial activity is caused by their actual inhibitory impact on the Malaria parasitic organism, not by RBC lysis. The tested compounds did not exhibit any antagonistic activity of saponin on red blood cells at the dosage in which the parasite is killed. This investigation demonstrates that the antimalarial compound is not toxic to normal, unaffected human blood cells. The hemolysis results for every tested chemical are displayed in (Fig. 3).

2.3. Computational study

2.3.1. Docking study. To rationalize the effectiveness of the designed hybrid scaffolds, new pyrimidine-tethered spirochromane-based sulfonamide derivatives **SZ9** and **SZ14** which showed promising activity *in vitro* were docked against falcipain-2 (3BPF) and falcipain-3 (3BWK) protein structures that were fetched from the RCSB Protein Database. For docking purposes, Autodock Vina has been employed to dock the prepared ligands (3D structures) in the protein's catalytic site.

The active pyrimidine-tethered spirochromane sulfonamide hybrids interacted with falcipain-2 and falcipains-3 target proteins with the formation of H-bonding along with π–π stacking interactions. The docking results are summarised in (Table 2) which displays the binding energy of the corresponding ligands. The calculated binding free energy for *in vitro* active compounds demonstrated that the entities **SZ9** and **SZ14** have shown a substantial binding affinity towards *Pf*FP-2 with energy varied from −9.4 to −5.7 kcal mol^{-1} while −9.8 to −7.5 kcal $mole^{-1}$ against *Pf*FP-3 when compared with the standard inhibitors of *Pf*FP-2(E64) and *Pf*FP-3(K11017) (Table 4).

As shown in (Fig. 4) the catalytic site's amino acid residue of the enzyme falcipains-2 connected with the ligand **SZ14** through hydrogen bonding between the carbonyl oxygen of the chromane ring of the ligand with the hydrogen of GLN36 and CYS39 at bond lengths of 2.95 Å and 2.37 Å correspondingly. The TRP206 residue interacted with the chromane benzene ring through π–π interactions for the ligands **SZ14** and **SZ9** (Fig. 4 and 5). Similarly, for both the ligands **SZ14** and **SZ9**, the GLY83,

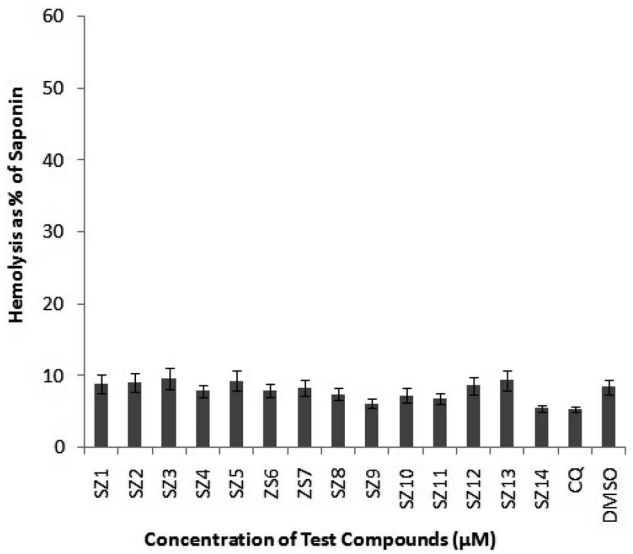

Fig. 3 Hemolytic experiment for the synthesized substances (SZ1-QS14) at a dose of 100 μM, while the negative and positive visuals were controlled using 0.5% of DMSO and 0.05% of saponin, respectively. With a standard deviation, the data represents the mean of two studies, each of which was conducted twice.

Table 4 Binding free energy of the active compounds (**SZ9** and **SZ14**) with *Pf*FP2 (PDB ID 3BPF) and *Pf*FP3 (PDB ID 3BWK) obtained from AutoDock Vina

Compound	Binding free energy (kcal mol^{-1}) *Pf*FP2 with PDB ID 3BPF	Binding free energy (kcal mol^{-1}) *Pf*FP3 with PDB ID 3BWK
SZ9	−9.4	−9.0
SZ14	−9.4	−9.8
E64	−5.7	—
K11017	—	−7.5

SER149, and ASN173 amino acid residue was associated with the carbon–hydrogen bonding interaction to the carbons of the piperazine, oxygen atom of sulfonyl groups, and the carbons atom of piperidine ring of spirochromane respectively (Fig. 4 and 5) while LEU84 and ILE85 were involved with the π–σ along with π–alkyl interaction with the phenyl ring of the sulfonamide portion correspondingly. The ASP234 was visualized to have interacted with the fluorine atom forming a halogen-type interaction along with π–anion interaction with the phenyl ring for the compound **SZ14** while for **SZ9** it shows only the π–anion interaction. Additionally, a hydrogen bonding in the middle of the fluorine atom of the **SZ9** ligand and the hydrogen atom of the ASN86 was visualized while such interaction was not displayed by entity **SZ14**.

The docking study of the active compounds with *Pf*FP-3 (3BWK) revealed that the compound **SZ14** exhibited a π–π interaction between the TYR93 and the benzene ring, three hydrogen bonding between the three fluorine atoms of CF_3 group with the GLY92 and HIS183 along with three carbon–hydrogen bond interaction: one within the GLY49 and nitrogen atom of the pyrimidine ring, the second between ASN182 and carbon of the piperazine ring, and third between TYR93 and one of the fluorine of the $-CF_3$ group (Fig. 6). Furthermore, an alkyl interaction was observed between the ALA184 and carbon atoms of the CF_3 group of the **SZ14** ligand. The binding site of the targeted protein also interacted with the compound **SZ9** with the formation of various interactions such as two π–π interactions between TRP215 and the phenyl ring of the ligand, the carbon–hydrogen bond interaction among the ASN182 and the carbon atoms of the piperidine ring. In addition, a π–alkyl interaction was viewed among the ALA166 and the benzene ring as well and another π–alkyl interaction was also noticed between PRO181 and the benzene ring of the spirochromane fragments in the binding site as imaged in Fig. 7.

To further investigate the aforementioned, the catalytic pockets of *Pf*FP-2 and *Pf*FP-3 were further docked with two

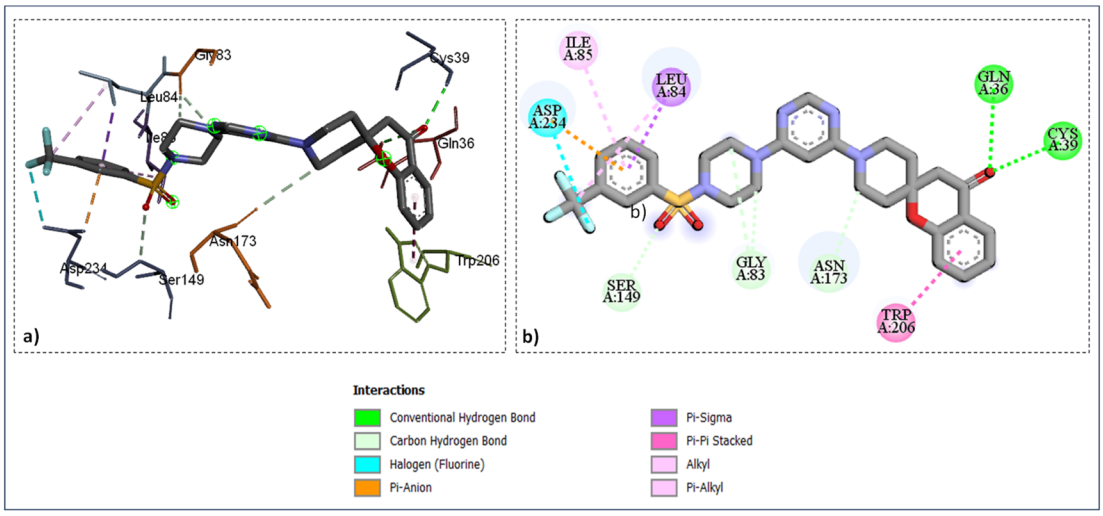

Fig. 4 Ligand docked protein interactions: (a) 3D binding pose showing the interaction of **SZ14** complexed with protein falcipain-2 (3BPF); (b) 2D binding pose showing the interaction of **SZ14** complexed with protein falcipain-2 (3BPF).

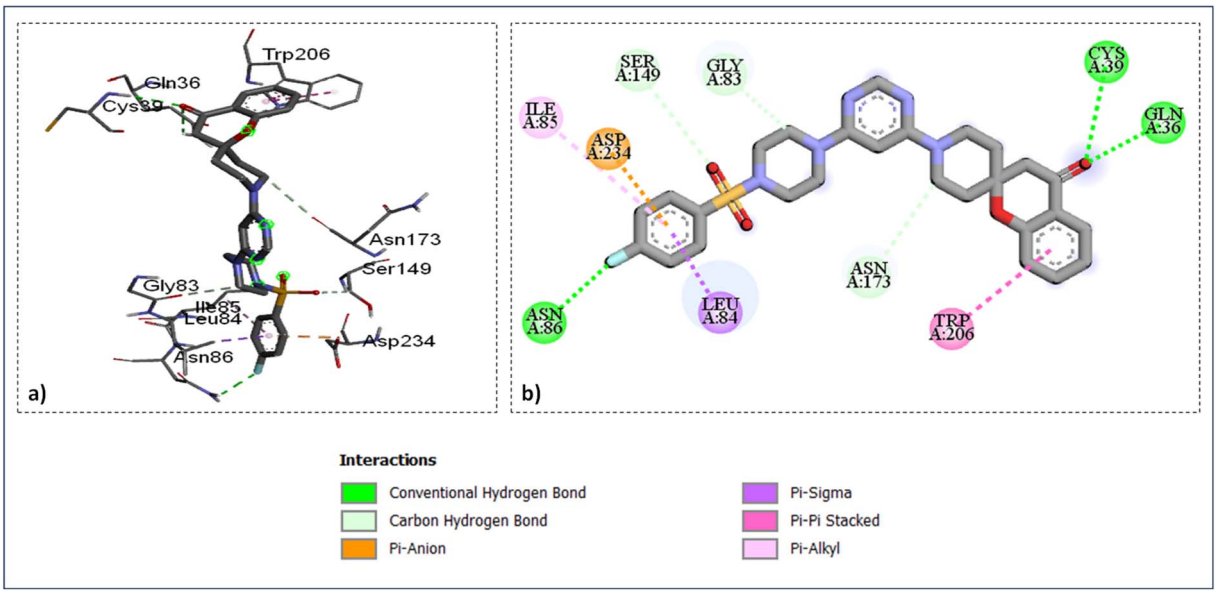

Fig. 5 Ligand docked protein interactions: (a) 3D binding pose showing the interaction of **SZ9** complexed with protein falcipain-2 (3BPF); (b) 2D binding pose showing the interaction of **SZ9** complexed with protein falcipain-2 (3BPF).

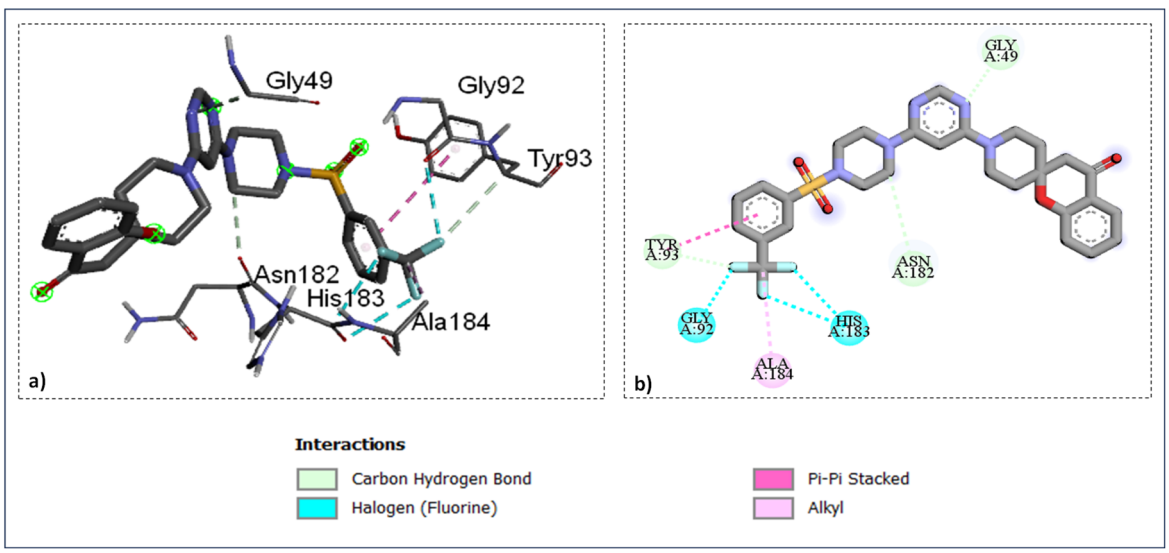

Fig. 6 Ligand docked protein interactions: (a) 3D binding pose showing the interaction of **SZ14** complexed with protein falcipain-3 (3BWK); (b) 2D binding pose showing the interaction of **SZ14** complexed with protein falcipain-3 (3BWK).

reference inhibitors, E64 and K11017 respectively. The ligands **SZ14** and **SZ9** demonstrate a higher binding affinity and easily occupy the receptor pocket compared to the reference molecules, as seen in (Fig. 8), which reveals how it accommodates the reference inhibitor molecules and active synthesized ligands. The proximity of the active compounds to the catalytic sites of both target proteins (*Pf*FP-2 and *Pf*FP-3) indicates the effectiveness and active involvement of the hydrophobic effective molecules interacting with the enzyme's catalytic site and subsequently suppressing enzyme activity.

2.3.2. Prediction of pharmacokinetic parameters. One of the most crucial tools in the development of a novel therapeutic molecule is the *in silico* pharmacokinetic and physicochemical analysis of tested compounds. Hence, utilizing the Qikprop module of the Schrodinger suit, *in silico* physiochemical characteristics and ADME estimations for potent substances (**SZ14** and **SZ9**) were performed to assess the drug-likeness of the tested hybrids, and outcomes of the study are displayed in (Table 5) and (Table 6). The guidelines of Lipinski's Rule of Five (Ro5) outline an important consideration for the prediction of drug-likeness[59] and the probability of a molecule having a high oral absorption was computed for the active compounds (Table 5), disclosing the findings with a maximum of two Lipinski's Rule breaches, falling within the acceptable range.[60] Thus, the

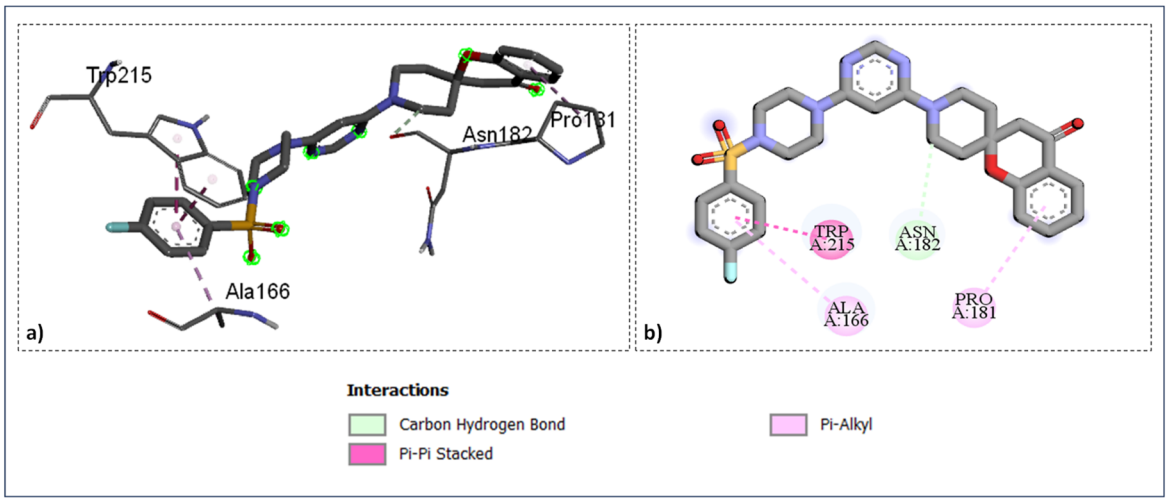

Fig. 7 Ligand docked protein interactions: (a) 3D binding pose showing the interaction of **SZ9** complexed with protein falcipain-3 (3BWK); (b) 2D binding pose showing the interaction of **SZ9** complexed with protein falcipain-3 (3BWK).

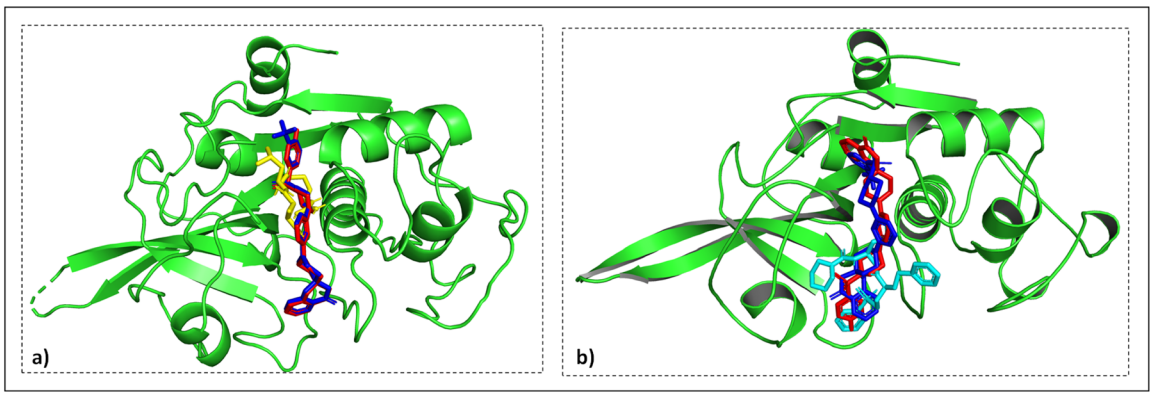

Fig. 8 Correlative visualizations of the inhibitors [E64(yellow) co-crystalized with *Pf*FP-2(3BPF) and K11017(cyan) co-crystalized with *Pf*FP-3(3BWK)] and the active entities **SZ14** (blue) and **SZ9** (red) bound to the active site of receptors: (a) ligands (**SZ14**, **SZ9**, and E64) bonded to the *Pf*FP-2(3BPF) active site; (b) ligands (**SZ14**, **SZ9**, and K11017) bonded to the *Pf*FP-3(3BWK) active site.

Table 5 Prediction of Lipinski RO5 for active compounds (**SZ9** and **SZ14**)

Compound	MW (<500 amu)	DonorHB (<5)	AccptHB (<10)	QPlogPo/w (<5)	N of violation (<2)	#Rotor (0–15)
SZ9	537.608	0	10.250	4.113	1	2
SZ14	587.616	0	10.250	4.938	1	2
CQ	319.876	1	4	4.537	0	8
PYM	248.714	4	3	1.793	0	4

study predicted that selected compounds are expected to exhibit drug-like characteristics and may be developed into oral active pharmaceuticals. Furthermore, for the active compounds (**SZ14** and **SZ9**), the important ADME parameters were also predicted and (Table 6) summarizes the results together with their permitted parameters. The predicted Percent Human Oral Absorption values for the two potent entities fell under the acceptable range (>80%). The drug's oral bioavailability parameter which is affected by the number of bonds that may be rotated (<15) and the polar surface area was also found in the acceptable limits for the aforementioned active compounds. To assess the intestinal absorption of the medicine, Caco-2 cell permeability (QPPCaco) was shown to be > 500 for the active molecules. For all investigated hybrids, the predicted values for human serum albumin binding (QPlogKhsa), brain/blood partition coefficient (QPlogBB), and aqueous solubility parameter (QP log S) were within the acceptable range. As a result, it was demonstrated that each active compound exhibited better

Table 6 Prediction of ADME parameters of active compounds (**SZ9** and **SZ14**)

Comp.	Percent human oral absorption (>80% – high & <25% – poor)	QPPCaco (<25 poor, >500 great)	QPlogBB (−3.0 to 1.5)	QPlogKhsa (−1.5 to 1.5)	QPlogHERG (below-5)	QPloS (−6.5 to 5)	PSA (70–200 Å)
SZ9	86.140	485.092	−0.997	0.305	−7.051	−6.743	101.854
SZ14	92.174	566.307	−0.812	0.548	−7.205	−7.878	102.657
CQ	100.000	1460.226	0.407	0.591	−6.329	−4.550	25.049
PYM	84.401	420.427	−0.768	−0.251	−4.286	−2.938	73.489

in silico physiochemical characteristics and ADME predictions, indicating that these compounds might develop into lead compounds with oral activity.

3. Conclusion

The present investigation addressed the designing of a set of new fourteen pyrimidine-tethered spirochromane-based sulphonamide derivatives and their chemical synthesis followed by their biological evaluation against malarial parasitic disease. **SZ14** displayed the strongest activity of all the synthesized compounds *in vitro* experiments against CQ-susceptible and CQ-resistant strains of *P. falciparum*, with IC_{50} values of 2.84 and 3.12 μM against both strains, respectively. Among all the tested compounds **SZ14** and **SZ9** were observed to possess antiplasmodial activity against *Pf*FP-2 and *Pf*FP-3 enzymes respectively. The selected compounds (**SZ9**, **SZ10**, **SZ11**, and **SZ14**) were also assessed for cytotoxicity *in vitro* and it was found that **SZ14** possessed the highest anti-malarial activity while presenting the least cytotoxic impact against the lung cancer A5489 cell line, indicating a strong safety index and a strong preference for the *Plasmodium* pathogen in contrast to human cells. Further, *in vitro* hemolysis was carried out with uninfected human erythrocytes for all the active compounds to establish biocompatibility, confirming these compounds possess specific anti-malaria activity that is not due to lysis of the human erythrocytes. The docking study for the active compounds (**SZ14** and **SZ9**) was performed with the FP-2 and FP-3 of the *P. falciparum* and stronger interaction was noticed with the amino acid unit at the active pocket of the targeted protein when compared to the known inhibitor of cysteine protease enzyme (FP-2 and FP-3). Moreover, the *in silico* physicochemical and ADME predictions described that these molecules possess good pharmacokinetic profiles, indicating that they might have a probability of being orally active lead molecules. Consequently, all the combined results from studies based on molecular docking, *in vitro* antimalarial assays, and predicted ADME profiling demonstrated that pyrimidine-tethered spirochromane-based sulphonamide derivatives could be further optimized for the development of potential antimalarial drugs.

4. Experimental

4.1. Chemistry

All the required commercially available small building blocks, solvents, and reagents utilized in the reaction were procured *via* commercial suppliers like Bld pharm, sigma Aldrich, Avra, and Spectrochem and used in the chemical synthesis without further purification. To check the reaction progress, thin layer chromatography (TLC) was developed on precoated aluminum sheets (Merck silica gel 60 F_{254}, 0.2 mm) by using a suitable system of solvents. For the visualization of developed chromatograms, UV light of a short wavelength was used. The Tanco melting point apparatus (ISO 9001: 2000 CO.) was used to obtain the melting of all the final products. Every synthetic intermediate and final product were isolated and pure through flash column chromatography by exploiting silica gel (200–240 Mesh) and the eluents were a binary mixture of ethyl acetate in petroleum ether and a binary mixture of methanol in chloroform. ^{1}H NMR and ^{13}C NMR of all the final compounds were reported on JEOL (JNM-ECZ 400S) 400 spectrometer. Relative chemical shifts (δ) in parts per million were measured in $CDCl_3$ solvent to the internal reference standard tetramethyl silane (TMS, δ 0.0, ^{1}H NMR) The molecular weight was confirmed by utilizing the mass spectra recorded on Agilent G6530AA (LC-HRMS-Q-TOF).

4.1.1. General synthetic procedure of *tert*-butyl 4-oxospiro [chromane-2,4′-piperidine]-1′-carboxylate (1). A reported method with few modifications was utilized to synthesize the *tert*-butyl 4-oxospiro[chromane-2,4′-piperidine]-1′-carboxylate (**1**).[61] Generally, 1-Boc-4-piperidone (7.30 g, 36.637 mmol) was mixed with a stirring solution of *ortho*-hydroxyacetophenone (5.00 g, 36.724 mmol) in methanol (30 mL). To this solution was mixed pyrrolidine (3.70 g, 4.27 mL, 52.022 mmol) and heated at 80 °C for 6–8 hours. Using thin-layer chromatography (TLC), the reaction's progress was tracked. After the reaction was over, the excess methanol was reduced in a vacuum and the resulting crude was purified through flash column chromatography using a binary mixture of EtOAc and pet-ether (10% EtOAc/pet ether to 15% EtOAc/pet ether) as eluent to furnish the product (1) as a solid(off-white). Yield: 8.95 g, 76.9%.

4.1.2. Synthetic procedure of spiro[chromane-2,4′-piperidin]-4-one (2).[41] The intermediate (1) (3.00 g, 1 eq., 9.452 mmol) was dissolved DCM (30 mL) in an RB (100 mL) flask and to this solution, TFA (6 mL, 8.3 eq., 78.407 mmol) was mixed drop by drop. At room temp, the reaction was set to stir for two hours. The reaction status was checked by TLC. After that, the reaction was neutralized by employing an aqueous NaOH solution (10N) and extracted with DCM. The organic part was dried over Na_2SO_4 (anhydrous) and concentrated in a vacuum. Finally, crude was purified using flash column chromatography

with methanol/chloroform (10–30%) as an eluent to afford the intermediate (2) as a colorless solid—yield: 1.50 g, 73.0%.

4.1.3. Synthetic procedure of 1′-(6-chloropyrimidin-4-yl) spiro[chromane-2,4′-piperidin]-4-one (3). Triethylamine (0.63 mL, 4.545 mmol) was poured into the stirred solution of 4,6-dichloropyrimidine (0.68 g, 4.598 mmol) in dry THF (40 mL) followed by the intermediate compound (**2**) (1 g, 4.602 mmol) was mixed part-wise, and left to stir at r.t. for overnight. The reaction's progress was tracked by TLC, and once the reaction finished, the solvent (THF) was reduced in a vacuum. Then water was poured into the resulting crude, layered with ethyl acetate, and brine-washed. Further, the ethyl acetate part was dried using sodium sulfate (anhydrous) and reduced in vacuum. Finally, the obtained mixture was purified by column chromatography utilizing EtOAc/pet ether (3–10% followed by 20%) as eluents to furnish the product (3). Yield: 0.70 g, 46.1%; melting point = 164–166 °C. ^{1}H NMR (400 MHz, $CDCl_3$) δ 8.36 (d, J = 1.0 Hz, 1H), 7.87 (dd, J = 7.8, 1.8 Hz, 1H), 7.51 (ddd, J = 8.2, 7.2, 1.8 Hz, 1H), 7.08–6.96 (m, 2H), 6.52 (d, J = 1.1 Hz, 1H), 4.17 (s, 2H), 3.41 (ddd, J = 13.6, 12.2, 3.0 Hz, 2H), 2.74 (s, 2H), 2.21–2.11 (m, 2H), 1.72–1.62 (m, 2H). ^{13}C NMR (101 MHz, $CDCl_3$) δ 191.29, 162.33, 160.42, 158.88, 158.35, 136.67, 126.87, 121.63, 120.79, 118.37, 101.60, 77.75, 77.48, 77.16, 76.84, 48.07, 39.84 (2C), 33.77 (2C).

4.1.4. Synthetic procedure of 1′-(6-(piperazin-1-yl)pyrimidin-4-yl)spiro[chromane-2,4′-piperidin]-4-one (4). To a stirred solution of piperazine (1.56 g, 18.110 mmol) and K_2CO_3 (5.00 g, 36.179 mmol) in dioxane (50 mL) was mixed the intermediate compound (**3**) (1.00 g, 3.032 mmol). The reaction was set for stirring at 80 °C for 10 h, on completion (TLC), the excess dioxane was reduced under vacuum. To the obtained crude was added water, extracted with chloroform, and dried using sodium sulfate (anhydrous), and the organic part was concentrated in a vacuum. Then the concentrated part was taken to purification with column chromatography employing MeOH/$CHCl_3$ (5–10%) solution to furnish the intermediate (**4**) as viscous orange liquid. Yield: 0.80 g, 70.1%. ^{1}H NMR (400 MHz, $CDCl_3$) δ 8.22 (d, J = 0.9 Hz, 1H), 7.86 (dd, J = 7.8, 1.8 Hz, 1H), 7.53–7.45 (m, 1H), 7.05–6.96 (m, 2H), 5.60 (s, 1H), 4.11–4.01 (m, 2H), 3.61–3.54 (m, 4H), 3.41–3.29 (m, 2H), 2.99–2.94 (m, 4H), 2.93 (s, 1H), 2.72 (s, 2H), 2.14–2.04 (m, 2H), 1.78–1.56 (m, 2H). ^{13}C NMR (101 MHz, $CDCl_3$) δ 191.67, 163.50, 163.07, 159.10, 157.64, 136.51, 126.75, 121.36, 120.84, 118.40, 81.59, 78.15, 77.46, 48.11, 45.42 (2C), 44.79 (2C), 40.00 (2C), 33.72 (2C).

4.1.5. General synthetic procedure of final targeted compounds (SZ1–SZ14). A stirred solution of the intermediate compound (**4**) (1.00 g, 2.642 mmol) in dried methanol (30 mL) was placed over an ice bath and maintained at 0 °C temperature. Then various sulfonyl chlorides including aromatic as well as aliphatic sulfonyl chloride (1.2 eq.) were mixed with the reaction mixture followed by stirring for 8 h. TLC was used to track the development of the reaction. Once the reaction was finished, the excess methanol was eliminated in a vacuum. The crude was pure through flash column chromatography using EtOAc/pet ether (10–30% followed by higher percent) as eluent to furnish the desired product as solid. Yield: 53.7–69.3%.

*4.1.5.1. 1′-(6-(4-((4-Nitrophenyl) sulfonyl) piperazin-1-yl)pyrimidin-4-yl)spiro[chromane-2,4′-piperidin]-4-one (**SZ1**).* Yellow solid; melting point = 235–237 °C; yield: 0.96 g, 64.4%. ^{1}H NMR (400 MHz, $CDCl_3$) δ 8.38 (d, J = 8.8 Hz, 2H), 8.17 (s, 1H), 7.94 (d, J = 8.9 Hz, 2H), 7.87 (dd, J = 7.8, 1.8 Hz, 1H), 7.55–7.45 (m, 1H), 7.07–6.94 (m, 2H), 5.55 (s, 1H), 4.14–3.95 (m, 2H), 3.74–3.65 (m, 4H), 3.40–3.27 (m, 2H), 3.17–3.08 (m, 4H), 2.71 (s, 2H), 2.14–2.05 (m, 2H), 1.71–1.57 (m, 2H). ^{13}C NMR (101 MHz, $CDCl_3$) δ 191.56, 163.02, 162.80, 159.02, 157.69, 150.45, 141.67, 136.57, 129.00 (2C), 126.79, 124.57 (2C), 121.45, 120.81, 118.36, 81.71, 78.01, 48.08, 45.67 (2C), 43.72 (2C), 39.92 (2C), 33.71 (2C). HRMS (ESI) in MeOH calcd for $C_{27}H_{28}N_6O_6S$ $[M + H]^+$: 565.1791, found: 565.1847.

*4.1.5.2. 1′-(6-(4-((2-Nitrophenyl)sulfonyl)piperazin-1-yl) pyrimidin-4-yl)spiro [chromane-2,4′-piperidin]-4-one (**SZ2**).* Greenish white solid; melting point = 142–144 °C; yield: 0.97 g, 65.1%. ^{1}H NMR (400 MHz, $CDCl_3$) δ 8.19 (s, 1H), 7.98–7.93 (m, 1H), 7.88–7.83 (m, 1H), 7.76–7.66 (m, 2H), 7.63–7.58 (m, 1H), 7.54–7.46 (m, 1H), 7.07–6.94 (m, 2H), 5.62 (s, 1H), 4.12–4.01 (m, 2H), 3.74–3.62 (m, 6H), 3.39–3.30 (m, 4H), 2.72 (s, 2H), 2.09 (d, J = 14.3 Hz, 2H), 1.76–1.52 (m, 2H). ^{13}C NMR (101 MHz, $CDCl_3$) δ 191.74, 163.00, 162.94, 159.06, 157.65, 148.49, 136.60, 134.13, 131.78, 131.08, 130.84, 126.74, 124.27, 121.42, 120.76, 118.41, 81.85, 63.76, 48.08 (2C), 45.60 (2C), 44.03 (2C), 39.94, 33.68 (2C). HRMS (ESI) in MeOH calcd for $C_{27}H_{28}N_6O_6S$ $[M + H]^+$: 565.1791, found: 565.1853.

*4.1.5.3. 1′-(6-(4-(Naphthalen-2-ylsulfonyl)piperazin-1-yl)pyrimidin-4-yl)spiro[chromane-2,4′-piperidin]-4-one (**SZ3**).* Light green; melting point = 196–198 °C; yield: 0.90 g, 60.0%. ^{1}H NMR (400 MHz, $CDCl_3$) δ 8.30 (br, 1H), 8.11 (s, 1H), 7.94 (d, J = 8.5 Hz, 2H), 7.89 (d, J = 8.4 Hz, 1H), 7.83 (dd, J = 7.8, 1.8 Hz, 1H), 7.70 (dd, J = 8.6, 1.8 Hz, 1H), 7.67–7.56 (m, 2H), 7.51–7.42 (m, 1H), 7.04–6.92 (m, 1H), 5.51 (s, 1H), 4.83–4.73 (m, 2H), 4.06–3.94 (m, 2H), 3.65 (t, J = 5.0 Hz, 2H), 3.34–3.22 (m, 2H), 3.10 (t, J = 5.1 Hz, 4H), 2.67 (s, 2H), 2.07–2.01 (m, 2H), 1.66–1.53 (m, 2H). ^{13}C NMR (101 MHz, $CDCl_3$) δ 191.58, 162.85, 162.67, 158.95, 157.52, 136.48, 134.96, 132.33, 132.17, 129.42, 129.22, 129.17, 129.08, 127.97, 127.76, 126.64, 122.83, 121.31, 120.68, 118.30, 81.54, 77.96, 47.98, 45.77 (2C), 43.61 (2C), 39.82 (2C), 33.57 (2C). HRMS (ESI) in MeOH calcd for $C_{31}H_{31}N_5O_4S$ $[M + H]^+$: 570.2097, found: 570.2187.

*4.1.5.4. 4-((4-(6-(4-Oxospiro[chromane-2,4′-piperidin]-1′-yl) pyrimidin-4-yl)piperazin-1-yl)sulfonyl)benzonitrile (**SZ4**).* Light green solid; melting point = 170–172 °C; yield: 0.97 g, 67.8%. ^{1}H NMR (400 MHz, CDCl3) δ 8.18 (s, 1H), 7.91–7.80 (m, 5H), 7.54–7.46 (m, 1H), 7.07–6.93 (m, 2H), 5.56 (s, 1H), 4.13–3.98 (m, 2H), 3.72–3.65 (m, 4H), 3.40–3.29 (m, 2H), 3.11 (t, J = 5.1 Hz, 4H), 2.72 (s, 2H), 2.14–2.00 (m, 2H), 1.73–1.61 (m, 2H).^{13}C NMR (101 MHz, $CDCl_3$) δ 191.62, 163.00, 162.79, 159.01, 157.66, 140.03, 136.57, 133.11 (2C), 128.37 (2C), 126.75, 121.43, 120.77, 118.37, 117.19, 116.95, 81.72, 78.01, 48.06, 45.67 (2C), 43.69 (2C), 39.91 (2C), 33.69 (2C). HRMS (ESI) in MeOH calcd for $C_{28}H_{28}N_6O_4S$ $[M + H]^+$: 545.1893, found: 545.1954.

*4.1.5.5. 1′-(6-(4-(Thiophen-2-ylsulfonyl)piperazin-1-yl) pyrimidin-4-yl) spiro[chromane-2,4′-piperidin]-4-one (**SZ5**).* Greenish white solid; melting point = 163–165 °C; yield: 0.87 g,

63.6%. ^{1}H NMR (400 MHz, $CDCl_3$) δ 8.17 (s, 1H), 7.85 (dd, J = 7.9, 1.8 Hz, 1H), 7.62 (dd, J = 5.0, 1.3 Hz, 1H), 7.55–7.45 (m, 2H), 7.13 (dd, J = 5.0, 3.7 Hz, 1H), 7.05–6.95 (m, 2H), 5.57 (s, 1H), 4.11–4.00 (m, 2H), 3.69 (t, J = 5.1 Hz, 4H), 3.39–3.27 (m, 2H), 3.10 (t, J = 5.1 Hz, 4H), 2.70 (s, 2H), 2.14–2.03 (m, 2H), 1.72–1.57 (m, 2H). ^{13}C NMR (101 MHz, $CDCl_3$) δ 191.67, 162.95, 162.83, 159.04, 157.62, 136.58, 135.51, 132.87, 132.67, 127.94, 126.75, 121.42, 120.77, 118.38, 81.70, 78.04, 48.08, 45.80 (2C), 43.56 (2C), 39.96 (2C), 33.69 (2C). HRMS (ESI) in MeOH calcd for $C_{25}H_{27}N_5O_4S_2$ $[M + H]^+$: 526.1504, found: 526.1571.

*4.1.5.6. 1′-(6-(4-((5-Chlorothiophen-2-yl) sulfonyl) piperazin-1-yl pyrimidin-4-yl) spiro [chromane-2,4′-piperidin]-4-one (**SZ6**).* Light green solid; melting point 79–81 °C; yield: 0.78 g, 53.7%. ^{1}H NMR (400 MHz, $CDCl_3$) δ 8.20 (s, 1H), 7.86 (dd, J = 7.8, 1.8 Hz, 1H), 7.50 (ddd, J = 8.8, 7.3, 1.8 Hz, 1H), 7.32 (d, J = 4.0 Hz, 1H), 7.06–6.93 (m, 3H), 5.59 (s, 1H), 4.06 (d, J = 13.6 Hz, 2H), 3.74–3.67 (m, 4H), 3.43–3.29 (m, 2H), 3.12 (t, J = 5.2 Hz, 4H), 2.72 (s, 2H), 2.17–2.04 (m, 2H), 1.73–1.60 (m, 2H). ^{13}C NMR (101 MHz, $CDCl_3$) δ 191.58, 163.02, 162.83, 159.07, 157.66, 138.01, 136.57, 133.77, 132.24, 127.37, 126.81, 121.46, 120.85, 118.40, 81.73, 78.07, 48.12, 45.78 (2C), 43.61 (2C), 40.01 (2C), 33.76 (2C). HRMS (ESI) in MeOH calcd for $C_{25}H_{26}ClN_5O_4S_2$ $[M + H]^+$: 560.1115, found: 560.1199.

*4.1.5.7. 1′-(6-(4-(Pyridin-3-ylsulfonyl)piperazin-1-yl)pyrimidin-4-yl)spiro[chromane-2,4′-piperidin]-4-one (**SZ7**).* Light green solid; melting point 144–146 °C; yield: 0.95 g, 69.3%.^{1}H NMR (400 MHz, $CDCl_3$) δ 8.97 (d, J = 1.5 Hz, 1H), 8.82 (dd, J = 4.9, 1.6 Hz, 1H), 8.16 (s, 1H), 8.03 (dt, J = 8.0, 1.7 Hz, 1H), 7.85 (dd, J = 7.9, 1.8 Hz, 1H), 7.54–7.45 (m, 2H), 7.05–6.92 (m, 2H), 5.56 (s, 1H), 4.22–3.89 (m, 2H), 3.69 (dd, J = 10.9, 6.4 Hz, 4H), 3.38–3.27 (m, 2H), 3.10 (t, J = 5.1 Hz, 4H), 2.71 (s, 2H), 2.12–2.04 (m, 2H), 1.69–1.59 (m, 2H). ^{13}C NMR (101 MHz, $CDCl_3$) δ 191.64, 163.01, 162.82, 159.04, 157.68, 153.79, 148.54, 136.58, 135.51, 132.39, 126.77, 123.98, 121.44, 120.80, 118.39, 81.74, 78.03, 77.48, 48.09, 45.62 (2C), 43.69 (2C), 39.93 (2C), 33.71 (2C). HRMS (ESI) in MeOH calcd for $C_{26}H_{28}N_6O_4S$ $[M + H]^+$: 521.1893, found: 521.1980.

*4.1.5.8. 1′-(6-(4-((2-Fluorophenyl)sulfonyl)piperazin-1-yl)pyrimidin-4-yl)spiro[chromane-2,4′-piperidin]-4-one (**SZ8**).* Pale yellow solid; melting point 88–90 °C; yield:0.88 g, 62.4%.^{1}H NMR (400 MHz, $CDCl_3$) δ 8.18 (s, 1H), 7.88–7.80 (m, 2H), 7.62–7.53 (m, 1H), 7.53–7.46 (m, 1H), 7.29 (dd, J = 7.6, 1.2 Hz, 1H), 7.24–7.16 (m, 1H), 7.06–6.95 (m, 2H), 5.58 (s, 1H), 4.14–4.01 (m, 2H), 3.74–3.60 (m, 4H), 3.40–3.27 (m, 2H), 3.27–3.21 (m, 4H), 2.71 (s, 2H), 2.14–2.01 (m, 2H), 1.71–1.60 (m, 2H). ^{13}C NMR (101 MHz, $CDCl_3$) δ 191.67, 163.02, 162.95, 159.05, 157.67, 136.58, 135.49 (d, J = 8.3 Hz), 131.42, 126.77, 124.75, 124.74, 121.42, 120.80, 118.40, 117.63, 117.41, 81.72, 78.06, 48.10, 45.49, 43.93 (2C), 39.94 (2C), 33.70 (2C). HRMS (ESI) in MeOH calcd for $C_{27}H_{28}FN_5O_4S$ $[M + H]^+$: 538.1846, found: 538.1913.

*4.1.5.9. 1′-(6-(4-((4-Fluorophenyl)sulfonyl)piperazin-1-yl)pyrimidin-4-yl)spiro[chromane-2,4′-piperidin]-4-one (**SZ9**).* White solid; melting point 160–162 °C; yield: 0.91 g, 64.1%. ^{1}H NMR (400 MHz, $CDCl_3$) δ 8.17 (s, 1H), 7.85 (dt, J = 7.8, 1.6 Hz, 1H), 7.80–7.71 (m, 2H), 7.55–7.44 (m, 1H), 7.26–7.15 (m, 2H), 7.00 (q, J = 7.9 Hz, 2H), 5.56 (s, 1H), 4.09–3.99 (m, 2H), 3.67 (t, J = 5.2 Hz, 4H), 3.32 (t, J = 11.3 Hz, 2H), 3.04 (t, J = 5.1 Hz, 4H), 2.71 (s, 2H), 2.08 (d, J = 13.7 Hz, 2H), 1.73–1.56 (m, 2H). ^{13}C NMR (101 MHz, $CDCl_3$) δ 191.63, 165.45 (d, J = 255.9 Hz), 162.96, 162.82, 159.02, 157.62, 136.56, 131.43, 130.58, 126.75, 121.42, 120.77, 118.37, 116.61 (d, J = 22.6 Hz) (2C), 81.65, 77.48, 77.16, 76.84, 48.06, 45.73 (2C), 43.62 (2C), 39.91 (2C), 33.67 (2C). HRMS (ESI) in MeOH calcd for $C_{27}H_{28}FN_5O_4S$ $[M + H]^+$: 538.1846, found: 538.1914. Elemental analysis: calculated C, 60.32; H, 5.25; N, 13.03; S, 5.96; found C, 60.23, H, 5.09; N, 12.75; S, 7.56.

*4.1.5.10. 1′-(6-(4-((3,5-Difluorophenyl) sulfonyl) piperazin-1-yl) pyrimidin-4-yl) spiro [chromane-2,4′-piperidin]-4-one (**SZ10**).* Off-white solid; melting point 196–198 °C; yield: 0.86 g, 58.6%. ^{1}H NMR (400 MHz, $CDCl_3$) δ 8.19 (s, 1H), 7.97–7.77 (m, 1H), 7.59–7.44 (m, 1H), 7.34–7.26 (m, 2H), 7.13–6.91 (m, 3H), 5.58 (s, 1H), 4.23–3.86 (m, 2H), 3.80–3.58 (m, 4H), 3.34 (t, J = 11.3 Hz, 2H), 3.11 (t, J = 5.1 Hz, 4H), 2.72 (s, 2H), 2.25–1.93 (m, 2H), 1.73–1.57 (m, 2H). ^{13}C NMR (101 MHz, $CDCl_3$) δ 191.62, 162.48 (dd, J = 267.4 Hz, 23.3 Hz), 159.02, 157.68, 138.88, 136.57, 126.77, 121.43, 120.79, 118.38, 111.29 (d, J = 27.8 Hz), 109.13, 108.89, 108.64, 81.68, 78.03, 48.08, 45.74 (2C), 43.64 (2C), 39.91 (2C), 33.69 (2C). HRMS (ESI) in MeOH calcd for $C_{27}H_{27}F_2N_5O_4S$ $[M + H]^+$: 556.1752, found: 556.1818.

*4.1.5.11. 1′-(6-(4-((3,4-Difluorophenyl)sulfonyl) piperazin-1-yl) pyrimidin-4-yl)spiro [chromane-2,4′-piperidin]-4-one (**SZ11**).* Pale green solid; melting point 170–172 °C; yield: 0.92 g, 62.7%. ^{1}H NMR (400 MHz, $CDCl_3$) δ 8.18 (s, 1H), 7.86 (d, J = 8.6 Hz, 1H), 7.55 (dq, J = 26.0, 8.5 Hz, 3H), 7.34 (q, J = 8.2 Hz, 1H), 7.07–6.91 (m, 2H), 5.57 (s, 1H), 4.14–3.99 (m, 2H), 3.81–3.59 (m, 4H), 3.40–3.26 (m, 2H), 3.11–3.04 (m, 4H), 2.72 (s, 2H), 2.33–1.87 (m, 2H), 1.80–1.46 (m, 2H). ^{13}C NMR (101 MHz, $CDCl_3$) δ 191.61, 162.98, 162.77, 159.01, 157.65, 150.38 (d, J = 261.59 Hz), 150.20 (d, J = 278.76 Hz), 149.09, 148.96, 136.56, 132.32, 126.74, 124.92, 121.41, 120.77, 118.60, 118.37, 117.75, 117.55, 81.67, 78.01, 48.06, 45.70 (2C), 43.61 (2C), 39.89 (2C), 33.67 (2C). HRMS (ESI) in MeOH calcd for $C_{27}H_{27}F_2N_5O_4S$ $[M + H]^+$: 556.1752, found: 556.1823.

*4.1.5.12. 1′-(6-(4-((3,5-Dimethylisoxazol-4-yl)sulfonyl) piperazin-1-yl) pyrimidin-4-yl) spiro[chromane-2,4′-piperidin]-4-one (**SZ12**).* Greenish white solid; melting point 182–184 °C; yield: 0.83 g, 58.4%. ^{1}H NMR (400 MHz, $CDCl_3$) δ 8.20 (s, 1H), 7.85 (dd, J = 7.8, 1.9 Hz, 1H), 7.56–7.44 (m, 1H), 7.00 (dd, J = 13.5, 7.8 Hz, 2H), 5.59 (s, 1H), 4.18–3.97 (m, 2H), 3.74–3.61 (m, 4H), 3.43–3.23 (m, 2H), 3.16 (t, J = 5.1 Hz, 4H), 2.72 (s, 2H), 2.63 (s, 3H), 2.39 (s, 3H), 2.21–1.94 (m, 2H), 1.80–1.49 (m, 2H). ^{13}C NMR (101 MHz, $CDCl_3$) δ 191.59, 174.09, 162.86, 162.69, 159.01, 158.00, 157.52, 136.58, 126.77, 121.45, 120.78, 118.38, 112.95, 81.71, 78.00, 77.48, 77.16, 76.84, 48.07, 45.14 (2C), 43.70 (2C), 39.96 (2C), 33.70 (2C), 13.14, 11.51. HRMS (ESI) in MeOH calcd for $C_{26}H_{30}N_6O_5S$ $[M + H]^+$: 539.1998, found: 539.2064.

*4.1.5.13. 1′-(6-(4-(Morpholinosulfonyl) piperazin-1-yl) pyrimidin-4-yl) spiro[chromane-2,4′-piperidin]-4-one (**SZ13**).* Light yellow solid; melting point 146–148 °C; yield: 0.95 g, 68.3%. ^{1}H NMR (400 MHz, $CDCl_3$) δ 8.23 (s, 1H), 7.86 (dd, J = 7.8, 1.8 Hz, 1H), 7.50 (ddd, J = 8.8, 7.2, 1.8 Hz, 1H), 7.06–6.96 (m, 2H), 5.61 (s, 1H), 4.14–4.04 (m, 2H), 3.77–3.68 (m, 4H), 3.67–3.60 (m, 4H), 3.42–3.29 (m, 6H), 3.27–3.20 (m, 4H), 2.72 (s, 2H), 2.16–2.06 (m, 2H), 1.74–1.61 (m, 2H). ^{13}C NMR (101 MHz, $CDCl_3$) δ 191.60, 162.96, 162.80, 159.03, 157.37, 136.58, 126.78, 121.45, 120.81,

118.39, 81.77, 78.03, 66.44 (2C), 48.10, 46.68 (2C), 46.18 (2C), 44.12 (2C), 40.05 (2C), 33.73 (2C). HRMS (ESI) in MeOH calcd for $C_{25}H_{32}N_6O_5S$ $[M + H]^+$: 529.2155, found: 529.2250.

*4.1.5.14 1′-(6-(4-((3-(Trifluoromethyl)phenyl)sulfonyl) piperazin-1-yl) pyrimidin-4-yl)spiro [chromane-2,4′-piperidin]-4-one (**SZ14**).* Off-white solid; melting point 138–140 °C; yield: 0.98 g, 63.2%. ^{1}H NMR (400 MHz, $CDCl_3$) δ 8.17 (s, 1H), 8.00 (s, 1H), 7.94 (d, J = 7.9 Hz, 1H), 7.90–7.80 (m, 2H), 7.70 (t, J = 7.8 Hz, 1H), 7.54–7.44 (m, 1H), 7.05–6.94 (m, 2H), 5.56 (s, 1H), 4.11–3.96 (m, 2H), 3.75–3.62 (m, 4H), 3.42–3.24 (m, 2H), 3.09 (t, J = 5.1 Hz, 4H), 2.71 (s, 2H), 2.14–2.00 (m, 2H), 1.73–1.56 (m, 2H). ^{13}C NMR (101 MHz, $CDCl_3$) δ 191.55, 163.06, 162.87, 159.05, 157.71, 137.03, 136.55, 132.61, 132.27, 131.94, 131.61, 131.00, 130.18, 129.85 (q, J = 3.03 Hz), 126.78, 124.73 (q, J = 4.04 Hz), 121.44, 120.85, 118.39, 81.71, 78.05, 48.11, 45.75 (2C), 43.69 (2C), 39.96 (2C), 33.74 (2C). HRMS (ESI) in MeOH calcd for $C_{28}H_{28}F_3N_5O_4S$ $[M + H]^+$: 588.1814, found: 588.1909. Elemental analysis: calculated C, 57.23; H, 4.80; N, 11.92; S, 5.46; found: C, 58.01; H, 4.36; N, 11.67; S, 7.07.

4.2. Biological study

4.2.1. Anti-plasmodial inhibition assays. The Malaria Research and Reagent Reference Resource Center (MR4), situated in the United States, provided the W2 and 3D7 strains of *P. falciparum*. While the *Pf*W2 strain is resistant to certain antimalarial drugs like pyrimethamine and chloroquine, the *Pf*3D7 is sensitive to all of the widely administered antimalarials. The antimalarial medication chloroquine and DMSO were acquired from the United States-based Sigma-Aldrich company. Human blood was extracted from healthy persons with a written agreement, in compliance with the procedures endorsed by the Institutional Ethics Committee of the Department of Cellular and Molecular Biology of the Institute. Red blood cells with 2.0 g L^{-1} of glucose, hematocrit of 2%, 300 mg L^{-1} of glutamine, 25 mg L^{-1} of gentamicin, 41.1 mg L^{-1} of hypoxanthine, and 0.5% AlbuMAX II were also present in the RPMI 1640 medium in which *P. falciparum* cells were grown at 37 °C with a gas mixture of 5% O_2 +5% CO_2 + 90% N_2. The culture was stained with Giemsa, and the smears were viewed using a light microscope with a resolution of ×100 to monitor the parasitic development. Parasites were synchronized by adding sorbitol (5%) to the ring stage cultures.[62] To conduct inhibitory tests, DMSO was used to dissolve the test compounds at a concentration of 25–30 mM whereas water was used to dissolve chloroquine at a 10 mM concentration. The compound stock underwent repeated dilution twice in 50 μL of RPMI 1640-albumax medium in a 96-well cell culture plate. The control wells accommodated either 0.5% DMSO solution or 500 nM chloroquine solution. The gas mixture is placed within a modular incubator chamber which was used to hold the plate after it was loaded applying 50 μL of the parasite solution (1% erythrocytes infected with rings at 4% hematocrit) for each individual. A 48–50 hour incubation period was then observed for the plate at 37 °C. Once the incubation period is ended, every single individual well-received 100 μL of lysis buffer (5 mM EDTA, 0.08% Triton X-100, 20 mM Tris-Cl 0.008% saponin, pH 7.5, with SYBR Green 1 at the dilution suggested by the manufacturer). The fluorescence of every single well was measured using a spectrofluorimeter equipped with automated microtiter plates (Molecular Devices, Flexstation) during a 30 minute incubation period at 37 °C. The test compound well fluorescence values were normalized as a percentage of the DMSO control's fluorescence value, plotted *versus* the test compound concentration, and then assessed to determine the half-maximal inhibitory concentration (IC_{50}).[63]

An investigation was executed to investigate the impact of a few compounds on the parasitic proliferation. The early ring stage 3D7 parasite of *P. falciparum* was dosed for 48 hours with substances (at 3 × IC_{50} concentration) or DMSO (Con, at 0.1%). Giemsa-stained smears were created from the test and control cultured before and following the treatment (48 hours). Photographs of the smears were observed and recorded using a 100× objective light microscope, Axio-Imager Z2.

4.2.2. Falcipain-2 and falcipain-3 enzyme inhibition assay. The enzyme inhibition procedure adopted which was previously used, FP-2 & FP-3 (30 nM) was incubated among distinct amounts of experimented molecules for 30 min at room temp. in sodium acetate solution (100 mM) and DTT (10 mM) of pH 5.5. A range of doses were produced from DMSO stock solutions, with the assay's highest DMSO dose being 1%. Once the substrate Z-Leu-Arg-AMC (benzoxycarbonyl-Leu-Arg-7-amino-4-methylcoumarin, Bachem AG) had been incubated for 30 minutes, it was mixed with the matching buffer until it reached a final strength of up to 25 lM. The difference in fluorescence was examined for 30 min excitation at 355 nM, emission at 460 nM, and ambient temp. through Spectrofluorimeter Molecular Devices, Flexstation having automatic microtiter plates. [20,64] The percentage inhibition results are presented on a log scale against the drug's concentration. To find out the related value of the half-maximal inhibitory concentration (IC_{50}) to prevent the targeted FP-2 and FP-3 enzymes, three separate, independent trials' % inhibition results were plotted against the concentration of the target molecule on a log scale graph. The Software GraphPad Prism, Version 3 (San Diego, CA), was exploited for the construction of the graphs.

4.2.3. Cytotoxicity study by MTT assay. The Cytotoxicity examination was performed through the MTT test which was employed to find out the blockage of the growth of Vero cells with the synthesized molecules employing Promega, Madison, WI, USA, Promega CellTiter 96 Non-radioactive Cell Proliferation Assay. [43,62,65,66] Following 72 hours of incubation at 37 °C, the viability was checked on the source of the Vero cells' cellular transformation of MTT into formazan, and the activity was evaluated with measurement of the intensity of absorption at 540 nm and then calculating the percentage of viable cells.

$$\%\ \text{Cell viability}\left[100 - \left(\frac{A_o - A_t}{A_o}\right) \times 100\right]$$

whereas: A_o stands for absorbance of cells treated by 0.1% DMSO media, A_t stands for absorbance of cells treated among diverse concentrations of the test.

Furthermore, the corresponding cytotoxicity was assessed with the lung cancer A5489 cell line using the previously

described standard procedure.[67] 10% foetal bovine serum supplemented Dulbecco's modified Eagle's medium (DMEM, Gibco, USA) was used to cultivate the cells. The test chemical compounds were administered at different dosages to cells seeded in a 160 μL medium at a density of 1 × 104 cells per well in a 96-well plate, which then underwent incubation for 24 hours at 37 °C. After being incubated for 24 hours, the medium was extracted, and MTT (25 μL) in 4 mmgg $mmLL^{-1-1}$ was introduced. This was accompanied by an additional 4 hour incubation period. After discarding the medium, DMSO (200 μL) was applied to liquidate the formazan crystals. Triplicates of the experiment were conducted, and the control wells were compared to evaluate the vitality of the cells. The Software GraphPad Prism, Version 3 (San Diego, CA) was applied for the determination of every test molecule's half-maximal inhibitory concentration (IC_{50}).

4.2.4. Hemolysis assay. Compounds' toxicity to host cells was assessed using the *in vitro* hemolytic evaluation, as previously mentioned, 68 the lead compounds' capacity to hemolyze human erythrocytes was checked. A 96-well cell culture plate containing RBC solution (200 μL) in PBS with 2% hemoglobin content was administered with the experimental compounds and 100 μM concentration of chloroquine. Use of DMSO (0.5%) and saponin (0.05%) as controls were chosen for the positive and negative images, respectively. Except for the saponin reaction, which needed 10 minutes to complete, every reaction was incubated for two hours at 37 °C. The absorbance of hemoglobin, a hemolysis marker, was measured (λ 540 nm) when the supernatants were transferred to a new 96-well tissue culture plate using Spectrofluorimeter Molecular Devices with automated microtiter plates. To plot the absorbance readings of the entities under investigation and the DMSO reactions presented as a proportion of the saponin reaction absorbance, Software GraphPad Prism, Version 3 (San Diego, CA) was employed.

4.3. Computational study

4.3.1. Docking protocol. A.pdb file containing the crystal structures of falcipain-3 (PDB ID 3BWK) and falcipains-2 (PDB ID 3BPF) was obtained from the Protein Database (**https://www.rcsb.org**). The ligand molecules were docked with the target proteins using AutoDock Vina (1.5.6 version). The .pdb file format of the ligands was prepared with the Marvin Sketch (ChemAxon version 19.18.0). PyMOL as well as Biovia Discovery Studio Visualizer v20.1.0.192 tool was utilised for the explanation of molecular interactions. The grid boxes were made sufficiently large to cover the protein and ligand interaction domains throughout the process of docking. To prepare the simulation box around the binding site of the ligand with the target protein, AutoGrid 4 was used. The simulation box centers for *Pf*FP-2 were set to $x = -59.722$, $y = -3.556$, and $z = -15.222$ and grid space was set to 1 Å with the grid size of 20 × 20 × 20 Å. Similarly, the simulation box centers for *Pf*FP-3 were set to $x = 6.222$, $y = -22.389$, and $z = 51.889$ and grid space was set to 1 Å with the grid size of 20 × 20 × 20 Å. Throughout the docking process, ligands, as well as proteins, were considered rigid, and the lowest binding energy or high binding affinity pose was further analyzed.

4.3.2. ADME analysis and physicochemical properties. To calculate the pharmacokinetic properties of ligands, the QikProp software module of the Schrodinger suite (LLC, New York, NY, 2021-2) was used. QikProp software uses the Jorgensen60 technique for the prediction of pharmacokinetic characteristics and descriptors like intestinal wall permeability, plasma protein binding, brain/blood partition coefficient, plasma protein binding aqueous solubility, brain/blood partition coefficient octanol/water partitioning coefficient, and others.

Abbreviations

P. falciparum	*Plasmodium falciparum*
FP-2	Falcipains-2
FP-3	Falcipains-3
ADME	Absorption, distribution, metabolism, and excretion
CQ	Chloroquine
FDA	Food and Drug Administration

Data availability

The data supporting this article have been included as part of the ESI.†

Author contributions

AR: docking studies, designing of the molecule, standardization of synthetic protocol, synthesis of compounds, analyzing NMR, compiling the results, and writing the original draft of the manuscript. SA: standardization of synthetic protocol, synthesis of compounds, reviewing, and editing the original manuscript. AS: characterizations, reviewing, and editing the original manuscript. SK: methodology. SF: reviewing and editing the original manuscript. TSP, JBD, and BCD: performing the antimalarial assay, enzyme inhibition assay, cytotoxicity, hemolysis, compilation of the results, analysis of the results, and writing related sections of the antimalarial activity. NH: conceptualization of the study, supervising the synthetic work, editing the manuscript, and arranging the funds for this project.

Conflicts of interest

The authors declare that they have no known competing financial interests or personal relationships that could have appeared to influence the work reported in this paper.

Acknowledgements

The author A. R. wishes to acknowledge the Ministry of Minority Affairs, Govt. of India for the research fellowship [No. f.82-27/2019(SA-III), UGC-Ref. No. 191620050863]. NH acknowledges SPARC (File No. SPARC/2019-2020/P2269/SL), the Ministry of

Education, Govt. of India for funding this project. TSP, JBD, and BCD are grateful to the principal and management of V. P. and R. P. T. P. Science College, Vallabh Vidyanagar for providing all the necessary research facilities and financial support for this research work.

References

1 M. A. Phillips, J. N. Burrows, C. Manyando, R. H. van Huijsduijnen, W. C. Van Voorhis and T. N. C. Wells, *Nat. Rev. Dis. Primers*, 2017, **3**, 17050.
2 A. F. Cowman, J. Healer, D. Marapana and K. Marsh, *Cell*, 2016, **167**, 610–624.
3 B. M. Greenwood, D. A. Fidock, D. E. Kyle, S. H. I. Kappe, P. L. Alonso, F. H. Collins and P. E. Duffy, *J. Clin. Invest.*, 2008, **118**, 1266–1276.
4 World Health Organization, *World Malaria Report 2023*, Geneva, 2023.
5 E. A. Ashley, M. Dhorda, R. M. Fairhurst, C. Amaratunga, P. Lim, S. Suon, S. Sreng, J. M. Anderson, S. Mao, B. Sam, C. Sopha, C. M. Chuor, C. Nguon, S. Sovannaroth, S. Pukrittayakamee, P. Jittamala, K. Chotivanich, K. Chutasmit, C. Suchatsoonthorn, R. Runcharoen, T. T. Hien, N. T. Thuy-Nhien, N. V. Thanh, N. H. Phu, Y. Htut, K.-T. Han, K. H. Aye, O. A. Mokuolu, R. R. Olaosebikan, O. O. Folaranmi, M. Mayxay, M. Khanthavong, B. Hongvanthong, P. N. Newton, M. A. Onyamboko, C. I. Fanello, A. K. Tshefu, N. Mishra, N. Valecha, A. P. Phyo, F. Nosten, P. Yi, R. Tripura, S. Borrmann, M. Bashraheil, J. Peshu, M. A. Faiz, A. Ghose, M. A. Hossain, R. Samad, M. R. Rahman, M. M. Hasan, A. Islam, O. Miotto, R. Amato, B. MacInnis, J. Stalker, D. P. Kwiatkowski, Z. Bozdech, A. Jeeyapant, P. Y. Cheah, T. Sakulthaew, J. Chalk, B. Intharabut, K. Silamut, S. J. Lee, B. Vihokhern, C. Kunasol, M. Imwong, J. Tarning, W. J. Taylor, S. Yeung, C. J. Woodrow, J. A. Flegg, D. Das, J. Smith, M. Venkatesan, C. V. Plowe, K. Stepniewska, P. J. Guerin, A. M. Dondorp, N. P. Day and N. J. White, *N. Engl. J. Med.*, 2014, **371**, 411–423.
6 A. M. Dondorp, F. Nosten, P. Yi, D. Das, A. P. Phyo, J. Tarning, K. M. Lwin, F. Ariey, W. Hanpithakpong, S. J. Lee, P. Ringwald, K. Silamut, M. Imwong, K. Chotivanich, P. Lim, T. Herdman, S. S. An, S. Yeung, P. Singhasivanon, N. P. J. Day, N. Lindegardh, D. Socheat and N. J. White, *N. Engl. J. Med.*, 2009, **361**, 455–467.
7 A. Uwimana, E. Legrand, B. H. Stokes, J.-L. M. Ndikumana, M. Warsame, N. Umulisa, D. Ngamije, T. Munyaneza, J.-B. Mazarati, K. Munguti, P. Campagne, A. Criscuolo, F. Ariey, M. Murindahabi, P. Ringwald, D. A. Fidock, A. Mbituyumuremyi and D. Menard, *Nat. Med.*, 2020, **26**, 1602–1608.
8 R. Leung-Toung, Y. Zhao, W. Li, T. Tam, K. Karimian and M. Spino, *Curr. Med. Chem.*, 2006, **13**, 547–581.
9 J. McKerrow, *Bioorg. Med. Chem.*, 1999, **7**, 639–644.
10 P. L. Olliaro and Y. Yuthavong, *Pharmacol. Ther.*, 1999, **81**, 91–110.
11 J. L. Siqueira-Neto, A. Debnath, L.-I. McCall, J. A. Bernatchez, M. Ndao, S. L. Reed and P. J. Rosenthal, *PLoS Neglected Trop. Dis.*, 2018, **12**, e0006512.
12 C. Teixeira, J. R. B. Gomes and P. Gomes, *Curr. Med. Chem.*, 2011, **18**, 1555–1572.
13 P. J. Rosenthal, *J. Exp. Biol.*, 2003, **206**, 3735–3744.
14 M. Marco and J. Miguel Coteron, *Curr. Top. Med. Chem.*, 2012, **12**, 408–444.
15 P. S. Sijwali, K. Kato, K. B. Seydel, J. Gut, J. Lehman, M. Klemba, D. E. Goldberg, L. H. Miller and P. J. Rosenthal, *Proc. Natl. Acad. Sci. U. S. A.*, 2004, **101**, 8721–8726.
16 P. S. Sijwali, J. Koo, N. Singh and P. J. Rosenthal, *Mol. Biochem. Parasitol.*, 2006, **150**, 96–106.
17 T. Conroy, J. T. Guo, N. Elias, K. M. Cergol, J. Gut, J. Legac, L. Khatoon, Y. Liu, S. McGowan, P. J. Rosenthal, N. H. Hunt and R. J. Payne, *J. Med. Chem.*, 2014, **57**, 10557–10563.
18 F. Shah, J. Gut, J. Legac, D. Shivakumar, W. Sherman, P. J. Rosenthal and M. A. Avery, *J. Chem. Inf. Model.*, 2012, **52**, 696–710.
19 T. M. Musyoka, A. M. Kanzi, K. A. Lobb and Ö. Tastan Bishop, *J. Biomol. Struct. Dyn.*, 2016, **34**, 2084–2101.
20 H. Li, J. Huang, L. Chen, X. Liu, T. Chen, J. Zhu, W. Lu, X. Shen, J. Li, R. Hilgenfeld and H. Jiang, *J. Med. Chem.*, 2009, **52**, 4936–4940.
21 P. M. Njogu, E. M. Guantai, E. Pavadai and K. Chibale, *ACS Infect. Dis.*, 2016, **2**, 8–31.
22 D. Rana, M. Kalamuddin, S. Sundriyal, V. Jaiswal, G. Sharma, K. Das Sarma, P. S. Sijwali, A. Mohmmed, P. Malhotra and N. Mahindroo, *Bioorg. Med. Chem.*, 2020, **28**, 115155.
23 A. Singh, M. Kalamuddin, M. Maqbool, A. Mohmmed, P. Malhotra and N. Hoda, *Bioorg. Chem.*, 2021, **108**, 104514.
24 H. Madhav, T. S. Patel, Z. Rizvi, G. S. Reddy, A. Rahman, M. A. Rahman, S. Ahmedi, S. Fatima, K. Saxena, N. Manzoor, S. Bhattacharjee, B. C. Dixit, P. S. Sijwali and N. Hoda, *Eur. J. Med. Chem.*, 2023, **258**, 115564.
25 F. W. Muregi and A. Ishih, *Drug Dev. Res.*, 2010, **71**, 20–32.
26 F. Simon, *Nat. Rev. Drug Discovery*, 2006, **5**, 881–882.
27 J. Walsh and A. Bell, *Curr. Pharm. Des.*, 2009, **15**, 2970–2985.
28 M. Jain, S. Vangapandu, S. Sachdeva, S. Singh, P. P. Singh, G. B. Jena, K. Tikoo, P. Ramarao, C. L. Kaul and R. Jain, *J. Med. Chem.*, 2004, **47**, 285–287.
29 S. B. Patil, *Heliyon*, 2023, **9**, e16773.
30 K. Singh and T. Kaur, *Medchemcomm*, 2016, **7**, 749–768.
31 R. T. Delfino, O. A. Santos-Filho and J. D. Figueroa-Villar, *J. Braz. Chem. Soc.*, 2002, **13**, 727–741.
32 K. A. Galal, A. Truong, F. Kwarcinski, C. de Silva, K. Avalani, T. M. Havener, M. E. Chirgwin, E. Merten, H. W. Ong, C. Willis, A. Abdelwaly, M. A. Helal, E. R. Derbyshire, R. Zutshi and D. H. Drewry, *J. Med. Chem.*, 2022, **65**, 13172–13197.
33 J. M. Coterón, D. Catterick, J. Castro, M. J. Chaparro, B. Díaz, E. Fernández, S. Ferrer, F. J. Gamo, M. Gordo, J. Gut, L. de las Heras, J. Legac, M. Marco, J. Miguel, V. Muñoz, E. Porras, J. C. de la Rosa, J. R. Ruiz, E. Sandoval, P. Ventosa,

P. J. Rosenthal and J. M. Fiandor, *J. Med. Chem.*, 2010, **53**, 6129–6152.
34 S. Chowdhary, Shalini, J. Mosnier, I. Fonta, B. Pradines, N. Cele, P. Seboletswe, P. Singh and V. Kumar, *ACS Med. Chem. Lett.*, 2022, **13**, 1068–1076.
35 M. Wang, T. Tang, R. Li, Z. Huang, D. Ling, L. Zheng, Y. Ding, T. Liu, W. Xu, F. Zhu, H. Min, R. Boonhok, F. Mao, J. Zhu, X. Li, L. Jiang and J. Li, *J. Med. Chem.*, 2022, **65**, 4156–4181.
36 R. Oliveira, R. C. Guedes, P. Meireles, I. S. Albuquerque, L. M. Gonçalves, E. Pires, M. R. Bronze, J. Gut, P. J. Rosenthal, M. Prudêncio, R. Moreira, P. M. O'Neill and F. Lopes, *J. Med. Chem.*, 2014, **57**, 4916–4923.
37 K. Hiesinger, D. Dar'in, E. Proschak and M. Krasavin, *J. Med. Chem.*, 2021, **64**, 150–183.
38 F. Lovering, J. Bikker and C. Humblet, *J. Med. Chem.*, 2009, **52**, 6752–6756.
39 M. Brindisi, S. Gemma, S. Kunjir, L. Di Cerbo, S. Brogi, S. Parapini, S. D'Alessandro, D. Taramelli, A. Habluetzel, S. Tapanelli, S. Lamponi, E. Novellino, G. Campiani and S. Butini, *Medchemcomm*, 2015, **6**, 357–362.
40 E. K. Schmitt, G. Ndayisaba, A. Yeka, K. P. Asante, M. P. Grobusch, E. Karita, H. Mugerwa, S. Asiimwe, A. Oduro, B. Fofana, S. Doumbia, G. Su, K. Csermak Renner, V. K. Venishetty, S. Sayyed, J. Straimer, I. Demin, S. Barsainya, C. Boulton and P. Gandhi, *Clin. Infect. Dis.*, 2022, **74**, 1831–1839.
41 B. F. Roberts, I. D. Iyamu, S. Lee, E. Lee, L. Ayong, D. E. Kyle, Y. Yuan, R. Manetsch and D. Chakrabarti, *Int. J. Parasitol.: Drugs Drug Resist.*, 2016, **6**, 85–92.
42 M. Jain, S. Nehra, P. C. Trivedi and R. V. Singh, *Heterocycl. Commun.*, 2003, **9**, 1.
43 T. S. Patel, J. D. Bhatt, R. B. Dixit, C. J. Chudasama, B. D. Patel and B. C. Dixit, *Arch. Pharm.*, 2019, **352**, 1900099.
44 V. R. Karpina, S. S. Kovalenko, S. M. Kovalenko, O. G. Drushlyak, N. D. Bunyatyan, V. A. Georgiyants, V. V. Ivanov, T. Langer and L. Maes, *Molecules*, 2020, **25**, 4485.
45 T. F. Mabasa, B. Awe, D. Laming and H. H. Kinfe, *Med. Chem.*, 2019, **15**, 685–692.
46 J. N. Domínguez, C. León, J. Rodrigues, N. Gamboa de Domínguez, J. Gut and P. J. Rosenthal, *Farm.*, 2005, **60**, 307–311.
47 S. Leeza Zaidi, S. M. Agarwal, P. Chavalitshewinkoon-Petmitr, T. Suksangpleng, K. Ahmad, F. Avecilla and A. Azam, *RSC Adv.*, 2016, **6**, 90371–90383.
48 A. I. Marealle, D. P. Mbwambo, W. P. Mikomangwa, M. Kilonzi, H. J. Mlyuka and R. F. Mutagonda, *Malar. J.*, 2018, **17**, 409.
49 M. Sinha, V. R. Dola, P. Agarwal, K. Srivastava, W. Haq, S. K. Puri and S. B. Katti, *Bioorg. Med. Chem.*, 2014, **22**, 3573–3586.
50 M. V. Papadopoulou, W. D. Bloomer, H. S. Rosenzweig, S. R. Wilkinson, J. Szular and M. Kaiser, *Eur. J. Med. Chem.*, 2016, **117**, 179–186.
51 D. J. Lowes, W. A. Guiguemde, M. C. Connelly, F. Zhu, M. S. Sigal, J. A. Clark, A. S. Lemoff, J. L. Derisi, E. B. Wilson and R. K. Guy, *J. Med. Chem.*, 2011, **54**, 7477–7485.
52 R. Sudhakar, N. Adhikari, S. Pamnani, A. Panda, M. Bhattacharjee, Z. Rizvi, S. Shehzad, D. Gupta and P. S. Sijwali, *Microbiol. Spectrum*, 2022, **10**, 3.
53 C. L. Yeates, J. F. Batchelor, E. C. Capon, N. J. Cheesman, M. Fry, A. T. Hudson, M. Pudney, H. Trimming, J. Woolven, J. M. Bueno, J. Chicharro, E. Fernández, J. M. Fiandor, D. Gargallo-Viola, F. Gómez de las Heras, E. Herreros and M. L. León, *J. Med. Chem.*, 2008, **51**, 2845–2852.
54 R. P. Brueckner, B. G. Schuster, K. C. Lasseter and E. T. Lin, *Am. J. Trop. Med. Hyg.*, 1998, **58**, 645–649.
55 F. Salas, J. Fichmann, G. K. Lee, M. D. Scott and P. J. Rosenthal, *Infect. Immun.*, 1995, **63**, 2120–2125.
56 P. Rosenthal, *Emerging Infect. Dis.*, 1998, **4**, 49–57.
57 S. C. Stolze, E. Deu, F. Kaschani, N. Li, B. I. Florea, K. H. Richau, T. Colby, R. A. L. van der Hoorn, H. S. Overkleeft, M. Bogyo and M. Kaiser, *Chem. Biol.*, 2012, **19**, 1546–1555.
58 J. Olson, *Bioorg. Med. Chem.*, 1999, **7**, 633–638.
59 C. A. Lipinski, F. Lombardo, B. W. Dominy and P. J. Feeney, *Adv. Drug Delivery Rev.*, 2001, **46**, 3–26.
60 B. C. Doak, B. Over, F. Giordanetto and J. Kihlberg, *Chem. Biol.*, 2014, **21**, 1115–1142.
61 T. Huang, J. Sun, Q. Wang, J. Gao and Y. Liu, *Molecules*, 2015, **20**, 16221–16234.
62 C. Lambros and J. P. Vanderberg, *J. Parasitol.*, 1979, **65**, 418.
63 P. S. Sijwali and P. J. Rosenthal, *Proc. Natl. Acad. Sci. U. S. A.*, 2004, **101**, 4384–4389.
64 W. Chen, Z. Huang, W. Wang, F. Mao, L. Guan, Y. Tang, H. Jiang, J. Li, J. Huang, L. Jiang and J. Zhu, *Bioorg. Med. Chem.*, 2017, **25**, 6467–6478.
65 R. Pignatello, G. Spampinato, V. Sorrenti, L. Vicari, C. Di Giacomo, A. Vanella and G. Puglisi, *Pharm. Pharmacol. Commun.*, 1999, **5**, 299–305.
66 J. D. Bhatt, C. J. Chudasama and K. D. Patel, *Arch. Pharm.*, 2017, **350**, 1700088.
67 K. Pal, M. K. Raza, J. Legac, A. Rahman, S. Manzoor, S. Bhattacharjee, P. J. Rosenthal and N. Hoda, *Eur. J. Med. Chem.*, 2023, **248**, 115055.
68 M. F. A. do Nascimento, T. F. Borgati, L. C. R. de Souza, C. A. Tagliati and A. B. de Oliveira, *Toxicol. Appl. Pharmacol.*, 2020, **401**, 115074.